Title
BUBBLE CHAMBERS

Author
Bradner, Hugh.

Publication Date
1960-05-23

UNIVERSITY OF CALIFORNIA

Ernest O. Lawrence Radiation Laboratory

BERKELEY, CALIFORNIA

DISCLAIMER

[illegible] of the [illegible] Therefore, I would like [illegible] to ask you to take [illegible] in hand, and give [illegible] comments [illegible]

I have been told that this paper should be pointed toward [illegible] who are not experts in the field. In fact, it was once said that [illegible] should assume the reader does not know anything at all about bubble ch[illegible] Of course, I have not tried to write for such an audience, since [illegible] that anyone who doesn't know a little bit about bubble chambers [illegible] not read [illegible]

Your extensive comments will be most welcome.

Sincerely,

Hugh Bradner

P.S. The deadline for submitting the manuscript is already [illegible] to have your comments very soon.

UCRL-9199

UNIVERSITY OF CALIFORNIA
Lawrence Radiation Laboratory
Berkeley, California

Contract No. W-7405-eng-48

BUBBLE CHAMBERS

Hugh Bradner

May 23, 1960

BUBBLE CHAMBERS

Contents

BUBBLE CHAMBERS[1]

Hugh Bradner
Lawrence Radiation Laboratory
University of California
Berkeley, California

May 23, 1960

I. INTRODUCTION

It has been five years since an article by Fretter (1), in this journal, described a new kind of nuclear particle detector, called the Bubble Chamber. During these years, bubble chambers have become the foremost detectors of particles from high-energy accelerators. Many Conference Reports and review articles on chamber design and data processing have been published. Extensive bibliographies by Ogden (2, 3) list work published before December 1958. The development and research effort in some laboratories has been extensive. The Alvarez group in Berkeley, for example, numbers more than one hundred people--including chamber operators, scientific assistants, engineers, and physicists--and costs 2 million dollars per year.

The field has already grown too large to be covered fully in a single article. This article a) indicates the great importance of bubble chambers and reviews the theory of their operation. b) discusses chamber designs and the handling of data. c) assembles some information useful to physicists in the planning of experiments. Emphasis in these latter sections will be on large bubble chambers, and especially on a large hydrogen bubble chamber.

The standard detectors of ionizing particles eight years ago were cloud chambers, counters, and nuclear emulsions. Each of these detectors had many forms, and each had limitations for use in high-energy nuclear physics, where new particles were being studied, and where the number of particles leaving an interaction frequently exceeded the number entering it.

Detectors that give images of charged-particle tracks are most valuable for investigating new or complex phenomena. High density is especially desirable if interesting events are to be produced in the detector. High spatial resolution is important. Cycling rates should be at least 10 per minute if the detector is to be used at an accelerator like the Bevatron or the Cosmotron. Very short time resolution, such as 10^{-8} second, would be desirable, so that many particles could be studied in a single accelerator pulse. The physicist often wants to determine velocity by ionization measurement, and momentum by track curvature in a magnetic field. He also needs to know the kind of nucleus in which a particle is produced or in which it interacts.

Nuclear emulsions afford high density and excellent spatial resolution, but can not yield momentum or even sign of charge, by track curvature in magnetic fields of 20 kilogauss. Emulsions contain such a mixture of complex nuclei that it usually is impossible to identify the interacting nucleus.

High-pressure hydrogen expansion cloud chambers, though presenting simple nuclei, have a cycling time of many minutes; so Shutt and others developed high-pressure hydrogen diffusion cloud chambers. However, diffusion chambers have a time resolution measured in seconds, the time for droplets to grow. Turbulence during droplet growth can limit the accuracy of spatial measurements. Furthermore, the sensitive depth of diffusion chambers is limited to about 3 inches, and the continuous sensitivity accentuates the problem of getting events without excessive background.

These shortcomings were widely recognized. It was also recognized that any detector of nuclear particles must operate by the triggering of some metastable energy source, since the particles passing through matter do not lose enough energy to be detected directly. But only Donald Glaser conceived that the localized effects of ionizing particles in a superheated liquid might give an imaging detector with the desired characteristics of sensitivity, rapid cycling, high density, and good spatial resolution. He developed a simple theory to describe the conditions under which a superheated liquid should be triggered into erupting upon the passage of an ionizing particle. This theory assumes that stable bubbles are formed when the net vapor pressure of the liquid, plus electrostatic repulsion of charge clusters, exceeds the surface tension of the liquid. Glaser tested his conclusions with a 1-cm.-diameter smooth glass vessel containing diethyl ether, which has a boiling point of 34.6° C. He raised the temperature of the liquid to 135°C, at a pressure of 300 psi, and then released the pressure, to leave the ether in a superheated condition. He reported (4) "in the presence of a 12.6-mc. CO^{60} source, the liquid in the tube always erupted as soon as the pressure was released, while when the source was removed, time delays between the time of pressure release and eruptive boiling ranged from 0 to 400 seconds, with an average time of about 68 seconds." The bubbles grew so rapidly that the ping of their shock wave striking the chamber walls could be heard. In 1953 Glaser reported success in photographing minimum-ionizing tracks of cosmic rays by triggering a flashlamp by a Geiger counter telescope(5). Good pictures in diethyl ether were obtained with flash delays of 10 μsec.

Counter-controlled expansion was apparently not possible, because the bubble nucleation centers de-excite too rapidly (6). Other physicists quickly realized the importance of this new detector, and began designing chambers for use with a variety of liquids. All early chambers were made with careful attention to smoothness and cleanliness of internal surfaces, since it was believed that bubbles would form at any rough places as soon as the chamber pressure was reduced, and that the expansion of these bubbles would repressurize the chamber and desensitize it before the ionizing particle could leave a track. Bubble chambers could not be made large enough to be really useful unless this limitation could be overcome. Early liquid hydrogen experiments by the Alvarez group showed a way to solve the problem. A 1-1/2-inch-diameter glass chamber was equipped with a fast pressure-release valve and a variable-delay light flash to attempt photography of proton recoil tracks from a Po-Be source (7). Tracks were observed, even when there was a large gas bubble in the chamber. Alvarez reasoned that the sudden release of pressure allowed bubbles to grow in the volume of the liquid before the large bubble at the wall could desensitize the chamber. Therefore, a large chamber could be made, without smooth clean surfaces, if the expansion were fast. The boldest and most important development of large chambers has certainly been the construction of a $14 \times 20 \times 72$-inch liquid hydrogen or deuterium chamber, under the direction of Alvarez at the Lawrence Radiation Laboratory.

The early history of the development of bubble chambers is very clearly described in Glaser's papers and in his review article in <u>Handbuch der Physik</u> (8). Comparisons of bubble chambers with other detectors can be found in Table 1 of that article and in the Geneva Atoms-for-Peace Conference article by Bradner and Glaser (9). As Glaser says, "the bubble chamber was invented because a detector of its properties was needed for experiments in high-energy physics."

II. BASIC IDEAS OF BUBBLE CHAMBER OPERATION

A. Thermodynamics

The operation of a bubble chamber can be understood with the aid of the PVT diagram, Figure 1, which shows representative isotherms for a fluid in the region near the critical point. If the pressure on a liquid in a rough-surfaced container is lowered slowly, gas begins to form when the isotherm intersects the liquid saturation curve, as at A in the figure. Attempts to decrease the pressure further merely produce more gas. The volume can be increased along the constant pressure line ACE until all the liquid is vaporized. It has been found that if the experiment is repeated, but with a very smooth, clean container, the pressure may be reduced beyond the point A, toward the point B on the ideal Van der Waals curve. This region is unstable; the liquid begins boiling abruptly, raising the pressure, and establishing the liquid-gas equilibrium mixture. Further expansion proceeds along a constant pressure line, as with the rough surface.

The time during which a liquid can be held in the unstable superheated state depends, among other things, on the degree of the superheat. In the absence of ionizing radiation it is possible to hold a wide variety of liquids at temperatures about 2/3 of the way from the boiling point to the critical temperature for several seconds.

B. Bubble Formation

The theories of liquid boiling consider whether small holes or vapor-filled bubbles tend to expand or collapse. The forces acting on an uncharged bubble in a liquid are the external pressure P and the surface tension σ trying to collapse the bubble, and the vapor pressure P_v trying to expand the bubble. It can be shown easily that bubbles smaller than a critical radius r_c collapse, whereas bubbles larger than the critical radius will grow. The critical radius is given by

$$P_V - P = \frac{2\sigma}{r_c} \quad . \tag{1}$$

We can think of the liquid as continually undergoing formation and collapse of tiny bubbles as a result of statistical thermal fluctuations. Increasing temperature increases the probability that a bubble exceeding critical size will be formed.

Glaser (10) reasoned that the passage of an ionizing particle could change the critical bubble size, since a cluster of charged ions with like sign may be trapped on the wall of a bubble, and increase the expansion force by their mutual repulsion. He predicted that a bubble carrying n_q like charges would grow in a liquid of dielectric constant ϵ, if the saturated vapor pressure exceeds the applied pressure by an amount

$$P_V - P \geq \frac{3}{2} \left(\frac{4\pi \sigma^4 \epsilon}{n_q^2 e^2} \right)^{1/3} \quad . \tag{2}$$

This formula has been successful in predicting the operating conditions for a wide range of bubble chamber liquids, if n_q is taken to be about 6. However, Glaser's Handbuch article gives several reasons for doubting the theory.

One of the most effective arguments results from observations of stopping α particles: The theory would require that 900 charges of the same sign must be deposited in a region 2×10^{-6} cm. in diameter. This charge concentration is greater than the maximum ionization density attained by a stopping α particle, even granting the possibility that all the opposite charges could separate. The total energy lost by the α particle is great enough to produce stable bubbles, but some other mechanism than charge clusters must be found for transferring the energy to the liquid.

Another serious argument against the charged-bubble theory comes from the observation that pure xenon does not produce bubble tracks, but works very well when 2 percent of ethylene is added. The failure can be understood by noting that pure xenon is a good scintillator: Most of the energy lost by an ionizing particle is used in ionizing and exciting the atoms of the liquid. Xenon is monatomic, and hence can not have rotational or vibrational degrees of freedom to de-excite the atoms by collisions of the second kind before they radiate their energy away from the local region of ionization. The addition of ethylene or other quenching agent furnishes molecules with the necessary degrees of freedom to absorb the radiation and convert it locally to thermal energy.

We can consider that an ionizing particle acts like a hot needle plunged into the bubble chamber liquid. Viewed microscopically, there are, of course, local fluctuations in the heat delivered to the liquid, because of variations in the energies of ions and δ rays. A theory of bubble formation by local heating has been developed by Seitz (11), who concludes that δ rays of about 1 kev deposit their energy in a small region of about 10^{-6} cm. radius, to explosively produce bubbles of larger than critical size in 10^{-10} sec. The number of δ rays per cm. of path with energy between E_1 and E_2 kilovolts is given by

$$n_\delta = \frac{153\, Z\, \rho}{\beta^2 A} \left(\frac{1}{E_1} - \frac{1}{E_2} \right), \tag{3}$$

where ρ is the density, A the atomic mass and Z the atomic number of the liquid, and β is the v/c of the particle. Hence Seitz' theory predicts that the bubble density at a given temperature should be proportional to β^{-2} rather than to specific ionization. Values of $\frac{1}{2}$ kev for E_1 and 1 kev for E_2 in equation 3 give correct bubble densities for normal operating sensitivity, viz., about 8 bubbles per cm. for a minimum-ionizing particle in a hydrogen bubble chamber. The operating sensitivity of a bubble chamber can be adjusted by varying the degree of superheat so as to give anything from a few bubbles per cm. for heavily ionizing particles to saturated tracks for minimum-ionizing particles. [illegible] the minimum necessary δ-ray energy E_1, but has little effect on E_2. Since E_2 is probably several times as large as E_1, the bubble density should be given approximately by $n_b \approx \beta^{-2} B(T)$, where B(T) is a function only of temperature for a given liquid.

C. Number of Bubbles per Unit Length of Track

Glaser, Rahm & Dodd (12) found experimentally that the number of bubbles per cm. from π^+ mesons and protons of velocity βc in propane follows a relationship, $n_b = A\beta^{-2} + B(T)$, in which A is constant, 9.2 ± 0.2, between temperatures of 55°C and 59.5°C. Below 55°C, the value of A decreases rapidly. B is a function of temperature only.

They found that bubble densities were not proportional to total ionization or to β^{-2}. However, Willis et al. have re-examined Glaser's data, using gap counting instead of bubble counting, to avoid bias from overlapping bubble images (13). They report that the data are in agreement with a β^{-2} proportionality, but they point out that the specific ionization in the measured region varies as $\beta^{-1.83}$, which can not be distinguished from β^{-2} with the available data. Similar studies by Blinov et al., Bassi et al., and Birss give results in agreement with a β^{-2} variation of bubble density vs. velocity (14, 15, 16). But their data are equally consistent with a bubble density proportional to specific ionization. Birss reports bubble densities proportional to β^{-2} for π mesons and protons, but the constants of proportionality differ from each other by a factor of about 2. Blinov et al. report a small increase in bubble density for highly relativistic electrons in propane. However, unpublished work at CERN and Brookhaven indicates that bubble densities do not show the expected relativistic increase. It is a puzzle.

D. Rate of Bubble Growth

After a bubble has become larger than the critical size, its subsequent growth is governed by the rate of evaporation of liquid from the bubble surface. The growth rate depends mainly upon the rate of heat transfer from the surrounding liquid, although the reduction of vapor pressure by evaporative cooling may not be negligible. Theoretical treatments have been given by Plessett & Zwick (17) and by Birkhoff, Margulies & Horning (18). In both studies the effects of surface tension and viscosity have been neglected, and applied pressure has been assumed constant. Theory and experiment both indicate that the relation between bubble diameter and time can be expressed as $d = F\sqrt{t}$, in which the value of F is strongly dependent on temperature and pressure. A disagreement between theory and experiment on the size of F has been reported (19); but there is doubt whether existing pressure measurements are accurate enough to provide a good test.

At Berkeley the hydrogen chambers are photographed 2 to 5 milliseconds after the particles enter the chamber. Bubbles are then about 0.3 mm. in diameter. The new hydrogen chamber at Brookhaven, with a different kind of expansion system, shows 0.3-mm.-diameter bubbles in as little as 0.1 msec. after the beam particles. Characteristic times for propane and xenon are about 1 msec. and 3 msec.

A bubble chamber review article by Bugg (20) contains an eight-page discussion of the theories of bubble formation and growth, with data on minimum temperatures, bubble energies, critical radii, surface tension, and heat capacities for hydrogen, deuterium, propane, and CF_3Br.

III. BUBBLE CHAMBER LIQUIDS

A. General

Bubble chambers have been made with any of a wide variety of pure liquids, liquid mixtures, and liquids containing dissolved gas. They range from hydrogen, with a density of 0.0586 and radiation length[2] of 1100 cm., to xenon, with density 2.3 and radiation length 3.7 cm.

Many hydrogen chambers are described in technical literature (22). Hydrogen is certainly the most significant liquid for use in high-energy physics, since it presents a target of pure protons in which most reactions can be unambiguously analyzed. This virtue is offset by serious cryogenic problems, since the operating temperature is about 28 °K. The heat of vaporization of hydrogen is 7.5 cal/cc. Deuterium, the lightest element containing neutrons has an operating temperature of 32 °K, and can easily be used in a chamber designed for hydrogen.

Helium bubble chamber designs have been described by Block and co-workers (23). Helium is the lightest atom that has nuclear spin 0. The cryogenic problems with helium are somewhat more severe than with hydrogen; the operating temperature is 3 to 4 °K. Heat shielding must be better since the heat of vaporization of helium is only 0.73 cal./cc. The range of operating pressures for He is from 4 p.s.i.a. to just above atmospheric pressure, in contrast to the 5 to 7 atm. required for hydrogen. Furthermore, helium is nonflammable.

Propane (C_3H_8) is the most commonly used organic liquid (24). A propane chamber operates at a temperature of 58 °C and a pressure of 21 atm. Since the radiation length is about 110 cm. the characteristic length for gamma-ray conversion is less than that of pure hydrogen by a factor of 10. The amount of hydrogen per unit volume in a propane chamber is greater by a factor of 1.38 than in a hydrogen bubble chamber. However unambiguous separation of hydrogen and carbon interactions in [illegible]

Propane chambers are very much easier to build and operate than cryogenic chambers. However, the fire hazard with propane is at least as severe as with hydrogen. Both liquid vapors are highly flammable. Propane will sink into trenches and holes, while hydrogen will rise to the ceiling.

Liquids heavier than propane are used for experiments in which production of electron pairs by gamma rays is of primary importance. The shortest radiation lengths have been obtained with xenon (3.7 cm) and tungsten hexafluoride (3.7 cm). Xenon bubble chambers of approximately 25-liter capacity have been built in Russia (25), and in the United States (26). A small chamber with tungsten hexafluoride has been constructed by Teem at California Institute of Technology (27). Since very short radiation lengths are not necessary with large bubble chambers, a number of people have investigated liquids with radiation lengths in the region of 10 to 20 cm. Today, the most satisfactory medium-heavy liquids appear to be the Freons (28), especially CF_3Br. Several of the Freons are inexpensive, nonflammable, and noncorrosive, and have convenient working ranges of temperature and pressure. Williams (29) summarizes the properties of several practical heavy liquids; and also discusses the problems of kinematic analysis in the heavy-liquid chambers when multiple Coulomb scattering severely limits the precision of momentum determination by magnetic curvature. Williams emphasizes that one disadvantage of the Freon chambers is their complete lack of hydrogen.

The insertion of lead plates in hydrogen bubble chambers has often been suggested as a way of combining short radiation length with the advantages of pure hydrogen. A single lead plate was installed for one run of the Berkeley 10-inch hydrogen chamber, and provisions have been made for putting lead plates in the 72-inch hydrogen chamber.

B. Dissolved Gas in Bubble Chambers

Hildebrand has found that 1% of helium, or small amounts of neon, can be dissolved into liquid hydrogen bubble chambers without significant changes in operating conditions (30). This technique may be useful in investigating the Panofsky effect. Hildebrand found that a concentration of one neon atom in 5,000 hydrogen atoms made no change in bubble chamber operating conditions, but completely suppressed the μ-catalyzed hydrogen fusion, and gave a muon-capture rate characteristic of pure neon.

C. Gas Bubble Chambers

Several experimenters have produced a completely different kind of chamber by using a supersaturated solution of gas in liquid. (31) Two possible advantages of this type of chamber are a lengthening of the sensitive time, and operation at more convenient temperature. On the other hand, image distortions from liquid motion may be severe, since the evolution of gas is slow compared with vapor bubble growth. Bugg (20) concludes that the dissolved-gas chamber is important only when the pure liquid would be unstable at the temperature required for vapor bubble formation. Methyl iodide is an example of such a liquid. The pure liquid must be heated to 210°C for normal bubble chamber operation, but it decomposes above 150°C. If an equal volume of propane gas is dissolved in methyl iodide, the mixture operates as a gas bubble chamber at 110°C.

D. Properties of some Bubble Chamber Liquids

Table I presents operating parameters of several common chamber liquids. The temperature and vapor pressure are given for the pre-expanded condition. The mean temperature is a normal operating value for "good tracks" of 10 to 20 bubbles per cm from a minimum-ionizing particle. The range of temperature indicates approximate limits from first detection of tracks to spontaneous boiling. The density applies to the expanded liquid at the time that tracks are formed; numbers are given without ~ for quantities that have been measured, or computed accurately from π- μ-e range measurements.

The expansion ratios are drawn from actual operating experience, and may include some expansion due to initial rapid bubble formation. Hence the listed expansion ratios are generally larger than the thermodynamic values. The times listed for flash delay refer to the time between the passage of ionizing particles and the exposure of the photograph. The optimum flash delay is sensitively dependent on the pressure in the expanded chamber. Radiation lengths were computed according to footnote 2 of this review paper. Additional characteristics of n-pentane, iso-pentane, and diethyl ether are given by Bertranza, Martelli & Zacutti (32). Data for tungsten hexafluoride and for mixtures of methyl iodide with propane are given by Williams (29). Properties of several freons are given by Bugg (28), and by Hahn et al. (33). Extensive surveys of bubble chamber liquids were presented by Kalmus, and by Hahn during a 1959 CERN symposium on heavy-liquid chambers (34, 35).

IV. DESIGN, CONSTRUCTION, AND OPERATION

A. General

A bubble chamber is merely a pressure vessel with glass windows, and a flash camera for photographing bubbles in the liquid after a pressure-release valve is operated. Usually a magnet surrounds the chamber so that particle momentum can be determined by measuring track curvature. The design of the chamber varies with the temperature and pressure characteristics of the liquid as well as the techniques chosen for illumination and pressure release.

B. Steinberger 12-Inch Propane Chamber

A description of this chamber illustrates many of the design features of warm chambers. Some details of the design were given by Eisler et al. (22); other information was obtained by private communication from Richard J. Plano (Columbia University). Figures 2 and 3 show a photograph and a schematic of the chamber, which is 12 inches in diameter and 8 inches deep. The cylindrical aluminum body is closed on both ends by herculite plate glass windows. The chamber is operated with these window surfaces vertical. Liquid propane is maintained at 57° C and 21 atmospheres pressure by heating elements wrapped around the chamber. A commercial regulator, operated from a thermocouple attached to the chamber, maintains constant temperature. The chamber is expanded and recompressed by motion of a nylon-reinforced rubber diaphragm in the 5-inch-diameter neck of the opening below the chamber. The volume between this diaphragm and a second one, lower down, is filled with low-viscosity oil, which provides thermal insulation. Compressed air actuates the lower diaphragm. The operation proceeds as follows:

1. The chamber is held at a pressure of 325 psig (gauge pressure)
2. An electronic time impulse from the Cosmotron initiates chamber

expansion. Approximately 10 msec is required for the chamber to come to equilibrium at the new pressure. Then the particle beam is introduced, and the lights are flashed approximately 1 msec later in order to photograph the bubble tracks in the chamber.

3. Recompression of the chamber follows.

The complete cycle lasts for about 30 msec.

The chamber is usually operated in a horizontal magnetic field of 13.4 kgauss.

The illumination of the chamber is achieved by a single GE FT-220 flash lamp, 60 inches from the chamber. A 12.5-inch-diameter lens of 30-inch focal length, mounted just behind the chamber, converges the light through the chamber to a point equidistant between the three camera lenses, which are 40 inches from the inside surface of the front chamber glass. Thus, light is scattered from the bubbles to produce the track images on a dark field background. The three lenses (Goerz-Artar of 100 mm focal length) are mounted at the vertices of a 10-inch equilateral triangle, giving a stereo angle to the center of the chamber of 13 degrees for each pair of views. The images, on 35 mm Linograph Ortho film, are 1/10 actual size.

C. Large Nonhydrogen Chambers

Although a number of groups are designing or building large nonhydrogen chambers, there is little literature available yet. Some data on these chambers are assembled in Table II.

D. Hydrogen Chambers

The range of normal operating temperatures and pressures for a number of hydrogen chambers (43) is shown in Figure 4. Two chambers are described here to illustrate techniques of hydrogen chamber design. Then alternative methods of illumination, expansion, temperature control, etc., are discussed.

Shutt 20-inch hydrogen chamber. The 20-inch hydrogen chamber of Shutt's group at Brookhaven (44) is an example of an instrument whose size and cost still permit design decisions to be made primarily on technical considerations. We will see in a later section how factors of cost affect the design of large chambers.

The Shutt chamber is an aluminum forging, with internal dimensions of 20 by 9 inches normal to the magnetic field, and 10 inches parallel to the field. Figure 5 shows the bare chamber. It must be suspended in an evacuated enclosure and surrounded by cold shields to minimize heat losses due to convection, conduction, and radiation. Shutt employs a conventional design of hydrogen chamber thermal barrier: a shield at liquid hydrogen temperature surrounds the chamber, and is in turn surrounded by a shield at liquid nitrogen temperature. This arrangement minimizes the radiative heat loads on the hydrogen supplies. Most of the heat load is discharged by boiling off relatively inexpensive liquid nitrogen.

The chamber has two vertical windows of 1.25-inch-thick tempered glass. The illumination is similar to the Steinberger chamber arrangement. Two large glass lenses, cut to 20-inch by 9-inch dimensions, focus the light to a point between the cameras. Four separate 35-mm cameras, mounted in a 9-inch square array about 40 inches from the middle of the chamber, take four photographs, 1/9 chamber size.

The straight-through illumination led Shutt to build his magnet without pole pieces. It requires 1.2 megawatts to produce a horizontal magnetic field of 17 kgauss uniform to ± 3 percent throughout the chamber. The copper coils of the magnet weigh 3.5 tons, and the iron return yokes weigh 20 tons.

The chamber expansion is controlled by a helium-operated piston near the top of the chamber neck. The complete expansion-recompression cycle is adjustable in pressure, and in time down to 10 msec. The temperature of the chamber is controlled by a pressurized reservoir of hydrogen making thermal contact with the aluminum forging. Hydrogen boils off at a rate of 5 to 6 liters per hour when the chamber is not pulsed. An additional 2 liters per hour is lost when the chamber is pulsed 30 times a minute. The very rapid piston expansion allows the liquid to be put actually under tension so that bubble growth is very fast. Good tracks have been obtained with expansion ratios as small as 0.8 percent, compared with values of 2 to 4 percent for most other hydrogen chambers. Flash delays are as short as 25 μsec, compared with 2 to 5 msec for most other hydrogen chambers. The low expansion ratio and short flash delay indicate that there is little boiling at the piston, and hence little repressurization of the chamber. It seems likely, from the short flash delays and the shape of the chamber, that track distortions will be very small. Preliminary measurements indicate that the accuracy of momentum determination on fast tracks may be limited only by multiple Coulomb scattering.

Although the temperature difference from top to bottom of the chamber is less than 0.1° C during any given pulse, the chamber sensitivity varies considerably from pulse to pulse. Sensitivity also depends upon the chamber pressure at the time when the particles arrive. Nevertheless, bubble counting will be valuable for identifying particles, especially when the beam pulse is of short duration.

Alvarez 72-inch hydrogen chamber. The large hydrogen bubble chamber at Berkeley is described in several hundred Radiation Laboratory Engineering Notes (3), and is summarized in papers by Gow at the 1958 Geneva U. N. Conference on Peaceful Uses of Atomic Energy and the 1959 CERN Instrumentation Conference (22, 45).

The total cost of engineering and construction was approximately \$2,000,000, including \$500,000 for a special bubble chamber building. About 65 man-years of effort were involved.

Figure 6 shows a cutaway model of the chamber and magnet. Figure 7 is a longitudinal cross section of the chamber. Figure 8 is a photograph of the chamber. The chamber is 72 inches long, 20 inches wide, and 14 inches deep. It has a single horizontal window on top, whose short axis is tilted 7.5° with respect to the horizontal. Hydrogen bubbles striking the top glass rise to the upper edge and are removed by a "gulper." The chamber body is a 6300-lb casting of stainless steel. The material is an austenitic steel similar to Al SL-316, but with lower molybdenum content. It was chosen for low permeability, high strength, and good ductility at liquid hydrogen temperature. The chamber has a refrigerated copper liner that also serves as an expansion-port plate. A large number of holes in the plate permit expansion and recompression over a large area without generating big vortices during recompression.

The chamber is supported from the top plate of the vacuum tank by means of a radiation shield of reinforced weldment at liquid hydrogen temperature. The shield has sufficient strength to contain the hydrogen that would be released if the window should fail. A liquid-nitrogen-temperature radiation shield surrounds both the chamber and the hydrogen shield.

Gasket seals of indium or lead are used throughout the low-temperature assembly. The 3/16-inch difference in expansion between glass and metal in cooling down to 28°K makes it impossible to seal the top window onto the chamber permanently. Therefore, the indium seals in this region are mounted onto an inflatable gasket (46) of flattened stainless steel tubing, which is left deflated until the chamber has been cooled to below liquid nitrogen temperature. Finally the seal is made by inflating the gasket with 500 p. s. i. of helium gas. Figure 9 is a cross section of the inflatable gasket. A vacuum vessel of mild steel encloses the chamber and the two low-temperature shields. The entire chamber assembly, supported as a unit inside the vacuum vessel, is inserted into a hole in the top of the magnet structure. The bottom of the chamber lies close to the bottom pole piece of the magnet. There is no top pole piece. The 200-ton 3 Mw magnet produces a field of 17 kgauss in the middle of the chamber. Low-conductivity water passing through the hollow square copper windings cools the magnet.

The complete structure can walk into different experimental areas on its feet. Parts of the refrigerator and vacuum equipment, most of the illumination power supply, extensive pressure-monitoring circuits, and the camera are mounted on the top platform of the magnet structure. Compressors and gas-purification system are in another room of the bubble chamber building. The refrigerator is a 1700-watt Joule-Thompson expansion unit. The temperature of the chamber is controlled by regulating the rate of flow of the refrigerating hydrogen around the chamber. A hydrogen vapor-pressure thermometer senses the temperature. The temperature regulation appears to be better than $\pm .05^{\circ}K$ at $28^{\circ}K$.

Approximately 3 days is required for cooling down from room temperature and filling with liquid hydrogen. The rate of temperature drop is limited by the allowed temperature gradient across the 5-inch-thick top window. Cooling starts with 5 p. s. i. g. hydrogen in the chamber and the support shield, in order to produce convective cooling of the glass. When the temperature has dropped to $25^{\circ}K$, very pure hydrogen is allowed to condense in the chamber. Impurities in the hydrogen must be kept below 1 part in 10^6 to prevent frost deposits which can spoil the quality of the pictures by condensing in visible amounts on the top glass and on reflectors at the bottom of the chamber.

The chamber is expanded through an 8-inch line by opening a modified Grove "flex-flow" boot valve into a 30 $ft.^3$ expansion tank at 17 p. s. i. a. The chamber is repressurized approximately 20 msec later by closing the expansion valve and opening a recompression boot valve from a 10-$ft.^3$ tank at 125 p. s. i. a.

Figure 10 is a schematic of the illumination system. Three special Edgerton Flash tubes of 50 watt-seconds each produce a flash lasting about 3/10 msec. (Flash tubes can be replaced with only a few minutes' interruption of chamber operation.) Three plastic aspheric condensing lenses of f/0.4 direct the light into the chamber. Dark-field illumination is achieved by use of "retrodirective coat hangers", which are discussed in Section V-I , below. Three Schneider Super-Angulon lenses give pictures of the chamber on a single strip of 46-mm film at 1/15 chamber size. The camera lenses are placed directly above the chamber, at three corners of a 20-inch square. The lens axes are perpendicular to the top glass. The lenses are stopped down to f/22 to bring the whole chamber depth in focus with optimum resolution. A data board displaying chamber operating conditions, times, beam counts, and roll and frame number is photographed simultaneously with each chamber exposure. A Polaroid Land camera, placed at the fourth corner of the 20-inch square, monitors the chamber operation. The light source and the camera box are maintained at a small positive pressure with clean gas, to prevent any escaping hydrogen from entering the regions of electrical contacts and high voltages.

A few measurements have been made on temperature gradients in the chamber and on the magnitude of turbulence and distortion. The temperature difference between bottom and top of the chamber can be held to less than 0.1°C. Measurements on the spurious curvature of 3.5-Bev/c π mesons with no magnetic field, and measurements on 1.6-Bev/c antiproton interactions at 18 kilogauss field, both showed a spurious radius of curvature of 160 to 200 meters. The rms uncertainty in radius of curvature due to multiple Coulomb scattering is about 600 meters for these π mesons and 280 meters for these antiprotons.

V. DESIGN CONSIDERATIONS FOR LARGE HYDROGEN CHAMBERS

A. General

The only existing hydrogen chamber larger than 60 liters is the 520-liter Alvarez chamber, described in the preceding section. Chambers of comparable size are being designed or constructed in Brookhaven (44), Great Britain (47), CERN (48), and the USSR (49, 50).

The new designs differ in some significant respects from the 72-inch chamber at Berkeley. Since large chambers are very expensive, it is worth while to discuss some of the design features and some of the reasons for their selection by the different groups.

Table III shows characteristics of various large chambers and of their associated magnets. Some of the features of these chambers are subject to change during development and construction, and should not be considered as definitely established.

B. Magnets

It is generally agreed that magnetic fields should be as strong as is economically possible, since the attainable momentum accuracy for a given length of track is about proportional to the magnetic field strength. The cost of obtaining fields higher than 16 to 20 kilogauss rises very rapidly because of the saturation of the iron at those field strengths. The field in the British chamber was originally planned to be 15 kgauss, but the value had to be lowered when the magnet dimensions were increased to accommodate the hydrogen shields. (47)

Uniformity of magnetic field throughout the chamber was of great importance in cloud chambers, but is not usually considered significant in large bubble chambers, where the event analysis is to be carried out in high-speed digital computers. The cost of computing the corrections for the nonuniform field in the analysis of 72-inch bubble chamber events is only $300 per year.

Bugg (20) has summarized some of the economic factors of magnet design, and Eaton & Hernandez (51) have reported on detailed considerations regarding the Berkeley 72-inch magnet. Figure ~~11~~ 13, from Eaton & Hernandez, shows the field in the 72-inch hydrogen chamber as a function of ampere turns for different weights of iron in the yoke.

C. Chamber Material

Chambers must be made of a metal that is strong and ductile at low temperature, in order to withstand the large impact forces of fast expansion and recompression. It is desirable to use a material with high tensile strength so that the chamber can occupy a minimum volume of magnetic field. The metal also should remain nonmagnetic at liquid hydrogen temperature. The composition of stainless steel castings must be controlled with particular care to obtain low permeability. The British have chosen machined aluminum because it satisfies these requirements (except strength), and is easy to fabricate. At one time they also felt that the high thermal conductivity of aluminum would be important in obtaining uniform temperature distribution of hydrogen in the chamber, but subsequent experiments with other chambers indicated that high thermal conductivity is probably not important. The only serious drawback to aluminum appears to be the large wall thickness that is required, with the resultant increase in magnet cost.

D. Chamber Windows

Borosilicate crown glass has been chosen for the Berkeley, Brookhaven, and British chambers. The thicknesses are 5 inches, 8 inches and 6 1/4-inches respectively. Fiducial marks can safely be etched, scribed, or sand-blasted on the inner surface, which is under compressional stress. Strength and fatigue tests on glass are reported by Kropschot (52). Tempered glass has not yet been used on large hydrogen chambers.

E. Gaskets

The differential thermal expansion between glass and metal requires that the window must be sealed to the chamber after the system is cooled, and unsealed before the chamber is warmed up. The Berkeley design of inflatable gasket with indium sealing surfaces has been very satisfactory.

F. Expansion Mechanisms

Ideally, chamber expansion should occur just early enough to make the chamber sensitive at the instant of beam arrival. Then recompression should take place as soon as the bubbles have been photographed. The expansion must start before the particles arrive, so that the reduced-pressure pulse can propagate at a rate of about 1000 m/sec throughout the hydrogen. Accordingly, about 5 to 10 msec is required to establish uniform sensitivity throughout the chamber. The time of arrival of the beam has a jitter of 1 or 2 msec. If the Bevatron rapid beam ejector is used, the beam particles can all arrive in less than 1 msec. With other modes of accelerator operation the beam can dribble into the bubble chamber over an arbitrary long period. The time for bubble growth requires a few additional milliseconds. All these times combine to give a total of about 20 msec, after which the pressure is reapplied rapidly. It is desirable to have the chamber pressure constant during the sensitive time, and reproducible from pulse to pulse, in order to get pictures with the same track sensitivity.

Barford (43) and Amiot et al. (53) have given extensive discussions of the existing expansion systems, and have suggested some improvements. Two basically different systems are used today. The liquid can be allowed to expand against a diaphragm or piston above the chamber at approximately 27° C temperature, as is done in the Shutt 20-inch chamber and proposed for the large Brookhaven and CERN chambers, or alternatively, large pipes can lead from the chamber up to a fast-acting valve at room temperature. This system is used in the large Berkeley chamber and is proposed for the British

It is, of course, a very difficult problem to obtain a satisfactory seal between the piston and cylinder in a liquid-expansion system over the wide range of temperatures. Shutt uses micarta piston rings to make a reasonably tight seal, but there is some leakage. Also abrasion produces visible quantities of dust, which would seriously reduce picture quality if the chamber windows were horizontal. Peyrou (54) reports on a 30-cm-diameter piston-expanded chamber, with similar excellent expansion ratios, and similar amounts of abrasion.

Steinberger has used a bellows in the expansion system of his 30-cm hydrogen chamber. This eliminates the problem of leakage and abrasion; but some workers feel that bellows can fatigue rapidly under conditions of pulse loading where high stresses may be concentrated in a few convolutions.

The outstanding-consideration in liquid expansion for large chambers is the reliability of the mechanical design, since repair of the piston or bellows can be expected to require warming the whole chamber up to room temperature, thereby interrupting chamber operation for at least a week. Liquid expansion systems do, on the other hand, have modest refrigeration requirements after the chamber has been filled with liquid hydrogen. The cost of refrigeration must be judged according to the reliability of the system, and weighed against possible interruptions of a bubble chamber run that costs \$10,000 per day.

All moving parts of the Alvarez chamber expansion system are at room temperature so that repairs can be made easily and quickly. The operation can be understood by referring to the schematic diagram of the 72-inch chamber, Figure 7. When the chamber is under pressure the expansion valve is closed and the liquid extends a small distance up into the expansion line. The higher regions of the expansion line contain gas at progressively warmer temperatures. To expand the chamber, the valve is momentarily opened to the expansion tank at 17 p. s. i. a. A few milliseconds later the valve is switched rapidly to the recompression tank at about 125 p. s. i. a. Finally the valve is closed, completing the cycle. Between expansions a recompressor re-establishes the appropriate pressure in the two tanks.

During the expansion cold gas moves up the expansion line and gains heat, which it delivers to lower regions during recompression. This undesirable heat load can be reduced by proper choice of expansion-line dimensions. Further reduction has been attempted by introducing a heat exchanger of copper wire mesh or similar high-heat-capacity material in the cold part of the expansion line. The detailed design of expansion line and heat exchangers must be fixed by trial, since the heat load is strongly dependent on the amount of turbulent mixing of warm and cold gas. Static and dynamic heat loads for three Berkeley hydrogen chambers are given by Gow (22). Gaseous expansion in large chambers requires a refrigerator that is larger by an order of magnitude than for liquid expansion, but a large refrigerator is usually wanted for initial cool-down of the chamber in either case.

G. Location of Windows

Reword?

A bubble chamber with a single window on the top affords the maximum safety if the glass should break. Also, a horizontal-window chamber allows beams of various momenta to be brought easily through the fringing magnetic field into the chamber in the desired location. Horizontal-window chambers offer distinct advantages in experiments involving polarized particles, since the polarization is generally determined by left-right asymmetry in the second scattering of a particle whose first scattering lay in the horizontal plane. The upper window can not be truly horizontal, but must be tipped several degrees so that bubbles can be swept away easily before being recompressed against the top glass. The geometry of separated beams

order needs to be changed?

introduces another consideration which may be very important for experiments on short-lived particles that require the bubble chamber to be put close to the accelerator: The angular separation between wanted and unwanted particles is characteristically about 1 milliradian. This produces such a small relative displacement of the particles that the separation is most effectively made in a vertical direction, while the fringing field of the accelerator focuses particles into a broad beam in the horizontal direction. Therefore the beam entering the bubble chamber is broad in comparison with its height. Such proportions are appropriate to a bubble chamber with the window on the top. This rectangular-cross-section beam can be rotated 90 degrees at the cost of several additional feet of quadrupole-type lenses. A disadvantage of horizontal windows is the possibility that dirt, or contaminating "frost" of solidified gas, can settle to the bottom of the chamber and deteriorate the quality of the image.

Chambers with windows on the side do not suffer from cleanliness problems. Shutt has indicated, for example, that the dust from abrasion of his piston system does not affect the quality of the pictures in his 30-inch chamber although they would make it completely unusable if the windows were horizontal. For some time it was thought also that uniform temperature throughout a bubble chamber could be maintained only by having a good heat conductor where the bubbles condensed at the top of the chamber. In the Berkeley chambers there was a great deal of difficulty in this respect, until automatic flap valves were installed to remove the bubbles and some liquid from the top of the chamber at each expansion. Both the Alvarez 72-inch chamber and the Shutt 20-inch chamber can be operated with less than 0.1° temperature difference throughout 90 percent of the chamber. Under these conditions the number of bubbles per unit length of a relativistic track is the same to within statistical accuracy at all points in the chamber.

The fringing fields of bubble chamber magnets bend the incoming particle beams in a way that will be awkward for long chambers with vertical windows. Since the experimenter wants the beam to travel the full length of the chamber, it may be necessary to use external magnets that bend and displace the beam vertically before it reaches the chamber. A horizontal-window chamber, on the other hand, can be aligned easily by rotating or moving the chamber.

None of the points mentioned above appears to be of completely overriding importance. Even the problem of introducing the beam into a chamber with horizontal magnetic field has a number of solutions. Shutt plans to use a bending magnet to deflect the particles at upward angles, and then to raise the chamber as much as 2 feet above beam height in order to get beams of momentum below 1 Bev/c into the chamber. The CERN chamber will incorporate a correcting coil placed directly in the side yoke and partly in the space between the main magnet coils, to allow beams of low momentum to enter the chamber undeviated.

H. Moving the Chamber

The entire structure of chamber and magnet must be provided with means for translation and rotation as required for the various particle beams. In addition, the Brookhaven chamber and the British chamber will need to be adjustable about 2 feet in height. Translation and rotation of the Berkeley chamber is accomplished by four hydraulically actuated feet. The height of the chamber is determined by a central support structure on which the magnet rests between translations. The Brookhaven magnet will move on wheels, either as a unit, or in separate halves, for removing the chamber. The British magnet will be provided with a hydraulic jacking system for adjusting the height, and will be moved horizontally on approximately 400 ball casters rolling on hard steel sheets. Peyrou reported that the CERN magnet will be moved on rails and rotated on a turntable (48).

Recently, however, he has stated informally that the magnet may be actuated in the same way as the Berkeley chamber. Hernandez has suggested that magnets could be moved by the simple and elegant mechanism of floating the magnet on a pad of compressed air, if the floor is sufficiently level.

I. Illumination

General. Bubble chambers must be illuminated with a short-duration high-intensity flash of well collimated light--intense enough to scatter a sufficient amount into the camera lens for photography.

Liquid hydrogen at chamber operating conditions has an index of refraction of 1.093 for light of 5300 angstroms (55). The intensity of light scattered at various angles from a spherical bubble can be calculated by geometrical optics, for bubbles that are large in diameter compared with the wave length (56, 49). The light intensity for various values of the refractive index is shown in Figure 12, taken from Barford. The rapid decrease of light with scattering angle implies that intense light sources are required, for scattering angles around 10 degrees. Scattering the light through 90 degrees is feasible for cloud chambers and heavy liquid bubble chambers, but not for hydrogen bubble chambers. The task of illumination is made even more difficult since bubbles are photographed at as early a moment as possible, in order that the tracks will have suffered a minimum displacement due to motions of the liquid. In any case, it is important to take the photograph while the bubbles are less than about 1/3 mm in diameter, so that bubble counting may be possible. Scattering angles as large as 10 degrees have been found to give satisfactory images with commercially available flashlamp sources.

Dark-field illumination, in which the only light reaching the cameras is scattered from the bubbles, produces pictures with satisfactory image contrast over a much wider range of illuminating intensity than the conventional light-field illumination.

Lighting is easy for very small chambers, but the possible designs of illumination and photography become progressively more restricted as the size of the chamber is increased. The ideal stereo system would use cameras pointing at the chamber on axes 90 degrees apart. Since dark-field illumination is desirable, straight-through illumination with the light source on the side opposite the camera is indicated. This leads to a design like the $2.5\times2.5\times10\text{-cm}^3$ chamber of Nagel, Hildebrand, & Plano, with four glass walls. (57) Such a system appears uneconomical with a chamber larger than about 6 inches. Middle-sized chambers are normally illuminated by a single flash on one side, and are photographed by two or more cameras, with axes parallel, on the opposite side of the chamber. The Steinberger propane chamber shown in Fig. 3 is a representative example of this type of illumination.

The CERN chamber and the British chamber are planned for modified forms of straight-through illumination.

The CERN chamber will use one flash lamp per camera lens, and will photograph bubbles with approximately 7 degrees deviation of the light. (48) The Berkeley chamber operates with a similar scattering angle. The British have designed their illumination for a scattering angle of approximately 2 degrees, in order to minimize the variation in image intensity with changes of illuminating angle. (47) Unfortunately, chromatic aberrations in the condenser systems that could be designed for this illumination would give variations in angle of about 3 degrees across the condenser aperture. Therefore the British will have to use monochromatic light, and hence will not gain the intensity that would have been expected from such small-angle illumination. They expect, in fact, that it will be necessary to use 650 joules to produce good images with "fairly fast film." By comparison, the Berkeley 72-inch chamber flash of 150 joules produces good images on linograph shellburst film with ASA rating of 100. The use of monochromatic light does, however, permit the British to eliminate reflection flares by applying a very-high-efficiency antireflection coating on the glass surfaces of the optical system and the chamber windows. Although straight-through illumination can be used with the largest chambers, considerations of magnet cost and of hydrogen safety in case of window breakage have led several groups to propose single-window designs for very large chambers, in which the cost of removing a pole piece or of adding an additional 10 inches of air gap can amount to $100,000.

Single-Window Illumination. The most direct way to illuminate a single-window chamber is to place a spherical Fresnel mirror in the bottom, and a light source outside, midway between the lenses of the cameras. Such a system has the serious disadvantage that light going into the chamber can be scattered from bubbles and produce ghost images below the chamber thereby reducing the number of tracks permissible in the chamber on each expansion by a factor of 2. One way to eliminate the ghost tracks is to cover the spherical mirror with small dimples or bumps a few mm in diameter and about 1 cm in radius of curvature. Bradner has made successful tests of this by pressing dimples into a polished aluminum plate with a polished steel ball. (58). Plano (41) and Barford (43) have also proposed this system. In spite of the heat-transfer advantages of a metal system, no one has undertaken to build a full-sized dimpled reflector, because of the difficulty of fabrication. Alvarez has proposed a one-window retrodirective illumination system, using a spherical Fresnel mirror in the bottom of the chamber, and Venetian blinds to eliminate ghost images (59). Other retrodirective materials--such as Scotch-light, corner reflectors, and machined grooves--of various shapes have been tested and abandoned because of insufficient collimation, manufacturing difficulties, or cost.

The ghost images in the 72-inch Berkeley bubble chamber have been avoided by using an array of 111 transparent Homolite plastic "coat hanger" reflectors each 22 inches long by 5/8 inch wide and 1 3/4 inches high, separated by 0.015 inch in order to allow heat transfer from the bottom of the chamber. Closer spacing causes spontaneous boiling at the edges of the reflectors. Figure ~~13~~ 15 shows cross-section drawings of the coat hangers for the 72-inch Berkeley chamber. In side view the reflectors are curved, with the radius equal to the distance to the flash source. In end view they are shaped so that light incident from the flash is focused onto an aluminized strip on the rear of the coat hanger and re-directed back at the source. Light scattered from a bubble before reaching the coat hanger is absorbed in the Homolite walls, which have been coated with "Luxorb" black, a material having the same index of refraction as Homolite. The top surface of each coat hanger has been made elliptical to produce a more even illumination throughout the chamber from the finite-sized source (60).

Although the coat hanger retrodirective illumination is a satisfactory single-window illumination system, it does give nonuniform illumination of bubble tracks, especially in the bottom two inches of the chamber. There is also a flare of at least 1 inch diameter on the top glass. If the glass and the coat hanger surfaces are allowed to get dirty, the flare size increases, and the photographic contrast decreases. However, careful attention to trapping of vacuum pumps and purifying of chamber hydrogen permits runs of several months duration without significant deterioration of image quality.

Several other illumination schemes have been discussed for single -window chambers. The Venetian blind system could be used by putting the flash lamps inside the actual chamber volume. Powell has built his 30-inch propane chamber this way, but the scheme does not seem to have been considered seriously for large hydrogen chambers because of the long time that would be required in warming up the chamber in order to replace lights. Schwemin has considered getting around the flash lamp problem by using electro-luminescent panels or phosphors with fast decay times, but has concluded that these approaches are impractical at present (61). Fiber optics lightpipes have also been proposed to carry the illumination from outside the chamber to the chamber bottom, but have been abandoned on considerations of cost and luminous intensity.

The ideal illumination system does not produce uniform intensity of light at the camera lens from all bubbles, since camera lenses reduce the intensity of off-axis images by a factor as large as $\cos^4\theta$. This off-axis vignetting is partially compensated in the Berkeley chamber, because the scattering angle of the light decreases as the position of the bubble gets farther off-axis. Additional compensation is made by adjusting the relative intensities of the three flash lamps that illuminate the separate regions of the chamber. Gray wedges and masks could be used to produce still greater image uniformity.

J. Photography

The parameters that must be considered in designing the photographic system for a bubble chamber include:

(1) The dimensions and depth of the chamber that must be photographed with approximately uniform resolution.

(2) The separation of the lenses.

(3) The distance from the chamber to the camera lenses.

(4) The focal lengths and resolution of available wide-angle camera lenses.

(5) The costs, speeds, resolutions and distortions of photographic film.

Wilson has discussed the depth of field for lenses photographing very small light sources in connection with design of cloud chamber optics (62). Good has carried out somewhat similar but simplified discussion of the optimum camera lens (63). Good proposes that we adjust the camera lens aperture so that the maximum diameter of the circle of confusion is equal in size to the diameter of the first diffraction minimum. By geometrical optics, the apparent size in the chamber of a point source at a distance h/2 beyond the center of the chamber is a circle of confusion of diameter $c \doteq ahp_o^{-1}$, as shown in Fig. 14. By physical optics considerations, a point source at the center of the chamber is imaged as a series of diffraction rings. The diameter of the central diffraction disk, measured in the chamber, is $d = \lambda p_o a^{-1}$. The diameter of the image from a point source should be approximately uniform throughout the depth of the chamber when these two terms are equal, i.e. when a^2h equals λp_o^2. Then the apparent object diameter would be about equal to $\sqrt{c^2+d^2}$, or $\sqrt{2\lambda h}$, quite independent of our choice of magnification or lens distance. In the Berkeley 72-inch bubble chamber, this equation predicts a limit of 0.7 mm diameter to the apparent size of a bubble in the chamber, independent of the distance from lens to chamber or of the magnification chosen. Usual practice in bubble chambers is to take the photograph when the bubble is approximately 0.3 mm diameter. Hence we would expect the apparent bubbles to be nearly 1 mm in diameter. Experience has shown that the above treatment is considerably in error because of the assumption that the diameter of the diffraction image is equal to the diameter of the central diffraction disk. The image is smaller by a factor of about 2, since bubble chamber photographs are taken on high-contrast film, which produces a black image only in the central part of the diffraction disk.

Although the simple theory indicates that the optimum lens opening for the 72-inch chamber cameras is f/27, the lenses can be opened up to f/22 before deterioration of the image anywhere in the chamber can be noticed. Normal film images in the 72-inch chamber are found to correspond to apparent bubble diameters of 0.5 mm in the chamber instead of the size predicted by Good's treatment.

The British propose to use two different sizes of film for their large chamber. Initially they will use unperforated 35-mm film in three separate cameras at demagnification of 16 with 3.25-inch focal length aerial survey lenses operated at aperture f/27. These cameras will be replaced later with units giving images at demagnification of 9 on 60-mm unperforated film with 6-inch focal length aerial survey lenses operating at f/45.

It may be possible to increase the useful depth of field by employing a lens with large spherical aberration, since it can be shown that the annular zone of the lens that brings a point into proper focus on high-contrast film produces a darker image than the integrated effect of the out-of-focus zones. (64)

Welford (65) points out that the ratio of circle of confusion to diffraction-disk diameter can be improved by covering the center of the lens aperture with a disk. A disk whose diameter is a fraction b of the lens aperture increases the depth of field by a factor $1/(1-b^2)$.

Welford's suggestion of using annular apertures may make it possible to increase the aperture of the British 6-inch lenses to about f/15 and obtain images of size limited only by the grain resolution of the film.

It will be noted that the focal length of the lens and the magnification of the image did not enter the expression for the apparent size of a bubble in the chamber. If we had ultrafine-grain distortionless film, and if all photographic lenses were equally good, then any convenient image size could be chosen, since all magnifications would allow the same precision of track reconstruction. A satisfactory expression for the resolution R of a picture taken on film with resolution F by a lens with resolution L appears to be $1/R^a = 1/F^a + 1/L^a$, with a value of a between 1 and 2. Either exponent leads to the reasonable conclusion that 15-fold demagnification is acceptable for film with resolution of 70 to 90 lines per mm. Larger images would require less precise coordinate measurement for the data reduction, and would decrease the errors from occasional serious distortions caused by film processing; but the difference in film cost between 10 diameters and 15 diameters demagnification on the 72-inch chamber was estimated to be $100,000 per year.

The transverse resolution of the optical system is determined by the resolution of a single lens and film, but the depth resolution is determined also by the geometry of the stereo reconstruction, and hence depends also upon the ratio of the camera lens separations to the distance from lens to camera. The depth resolution is always poorer than the transverse resolution. For perfect lenses it can be shown that the depth resolution improves as the lenses are moved closer to the chamber. A practical limit is set by the quality of the available wide-angle photographic lenses, in which the resolution is normally about 20 percent less than the resolution of the theoretically perfect lens. The 72-inch chamber uses Schneider super angulon lenses operating out to a maximum angle of 34 deg.

Although two lenses are sufficient to establish stereo geometry, a third lens is almost always added in order to speed up stereo reconstruction. A simplified expxplanation is as follows: Let us establish x, y, and z axes on each of two stereo images, with the z axis of each film perpendicular to its surface and passing through the optical axis of its lens, the x axis lying along the line between the two camera lenses. Then any arbitrarily chosen bubble will have the same y coordinate in both images. We do not have to identify the bubble on both images in order to make the geometrical reconstruction; we can make coordinate measurements on an arbitrary spot on the track in one view, and can find the appropriate x coordinate in the other view by y interpolation between near-by track coordinates in that view. The accuracy of this interpolation decreases as the direction of the track approaches the x axis, and it would be necessary to make coordinate measurements on corresponding bubble images to get 10-micron accuracy for tracks that lie closer than about 15 degrees to the x axis. If a third lens is placed at the vertex of an equilateral triangle or a corner of a square, it is always possible to find two views in which a track makes a large enough angle to the axis that bubble matching is unnecessary.

The use of four or more lenses would help eliminate occasional ambiguities in the photographs, or would permit focusing more sharply in restricted regions of the chamber, but the cost of film argues strongly against using more than three images.

VI. PRESENT LIMITATIONS TO BUBBLE CHAMBER OPERATION

A. Repetition Rate

The recycling rate of bubble chambers is limited purely by mechanical and thermodynamic factors. The cycling rate of most bubble chambers has been chosen to match the pulse-repetition rate of the high-energy accelerators for which they were intended. Kuznetsov _et al._ have built a Freon chamber to cycle 10 times per second for cosmic-ray research (66). At these very high rates there still appear to be some unsolved problems of removing the bubbles before the next expansion.

B. Track Distortion

A track image may be displaced from true track position by liquid motion subsequent to the bubble formation or by aberrations introduced in the mixing of liquids at different temperatures with unequal indices of refraction. The actual displacement of the bubbles can be reduced by shortening the light delay or by reducing the magnitude of the liquid motions. Two counter-rotating eddies in hydrogen, 12 cm in diameter and carrying liquid at the rate of 1 cm per second, can distort the track of a 1-Bev/c particle as much as the multiple Coulomb scattering. Donaldson and Watt point out that the half-time for decay of a vortex varies as the square of the vortex radius and is 13 minutes for a 2-cm-radius vortex in liquid hydrogen (67).

In addition to the gross distortions of track curvature mentioned above, there are short-wave-length wiggles which increase the root-mean-square deviation of the measured points from a smooth curve. This deviation σ_{xy}, referred to the horizontal plane in the 72-inch bubble chamber, is characteristically 60 microns or 1.2 apparent bubble diameters, for 30-inch-long tracks. Preliminary measurements of sample film from Peyrou's 30-cm hydrogen chamber and Shutt's 20-inch hydrogen chamber gave values of 30 to 50 microns for σ_{xy}. In all three cases, multiple Coulomb scattering would produce values of σ_{xy} nearly as large.

C. Number of Tracks per Picture

The number of beam tracks that can be permitted to go through a bubble chamber for a single picture is limited by the danger of getting ambiguous events, in which it is not possible to say definitely which reaction products are associated. Although 100 or 200 tracks can be used safely in cloud chambers, the higher density of bubble chamber liquids ordinarily limits the number of tracks to 20 or 30. This number probably could be increased by dribbling a beam into bubble chambers over an extended period of time, and then distinguishing associated tracks by the differences in bubble size. However, it seems clear that the time required to look for events in a picture would increase faster than the number of tracks, and hence, this technique is of questionable value as long as data analysis is slower than the rate of data accumulation.

D. Time Resolution

The time resolution of the bubble chamber as determined from bubble size is measured in tens or hundreds of microseconds. The time resolution as determined from the distance that particles travel before decaying is about 3 mm, or 10^{-11} second without relativistic time dilation.

E. Momentum Resolution

Momentum determination by measurements of track curvature in a magnetic field can never exceed the accuracy limit set by multiple Coulomb scattering (see Section VIII B). In several hydrogen chambers, momentum errors on relativistic tracks are less than twice this limit.

F. Speed of Analysis

The steps in analysis of bubble chamber pictures are described in the following section. It does not appear likely that an average rate greater than 300 events per day will be reached by improvement of the present system. Significantly higher rates can be achieved only by developing automatic character-recognition devices as well as fast measuring and computing techniques.

VII. ANALYSIS OF EVENTS

A. General

The analysis of bubble chamber events ordinarily requires stereo reconstruction of the trajectories of all particles involved, followed by a computation of the momentum balance and energy balance. Two-lens stereo photography permits this reconstruction if measurements are made on the same bubbles in the two views. Much more rapid stereo reconstruction can be done without bubble matching, on tracks that are at angles of more than about 15 degrees to the line between the camera lenses. For this reason three cameras are ordinarily located on the vertices of equilateral triangles of three of the corners of a square.

Analysis picture measurements can yield a comprehensive description of the event. The curvature of the track in the magnetic field is a measure of momentum ÷ charge; the direction of the curvature indicates the sign of the charge; the number of bubbles per unit length gives the velocity of the particle if its charge is known; the range of a particle that stops in the liquid gives the energy, if the particle mass is known; the change of curvature with distance can establish mass if measurements are sufficiently accurate, and if multiple Coulomb scattering is small enough. Energetic delta rays can give some information on the velocity of the particles.

In addition to observing tracks of charged particles; it is also possible sometimes to detect neutral particles by energy-momentum balance, or by observing charged decay fragments, or by observing secondary interactions that involve charged particles.

The frequent appearance of inelastic processes in high-energy physics usually demands that the trajectories of the particles be reconstructed with the highest possible accuracy. The geometrical problems of reconstructing an event in a bubble chamber are similar to the problems encountered in the analysis of cloud chamber photographs, but the reconstruction is complicated by the fact that the liquid has an index of refraction differing from unity. Furthermore, camera optics are usually wide-angle, and therefore corrections for the chamber windows are nonlinear. In addition, the magnetic fields in some chambers are very nonuniform.

The development of systems, apparatus, and computer programs for data reduction has been summarized in the reports of a number of conferences in Geneva (68, 69, 70). The greatest effort has been made by the group under the direction of Bradner in connection with the hydrogen chambers at Berkeley. Their system is described in Lawrence Radiation Laboratory Engineering notes (3) and in papers by Bradner and Solmitz (71, 72).

B. Need for Rapid Analysis

The review article by Fretter (1) in this Journal pointed out the difficulty of analyzing events with the necessary speed from high-pressure diffusion cloud chamber experiments at the Cosmotron. Physicists recognized that the number of interesting interactions in a bubble chamber would be even greater, by almost two orders of magnitude. The cost of developing and carrying out the data reduction for bubble chambers has been comparable to the cost of developing and operating the chambers.

The following discussion is based largely on the work with hydrogen bubble chambers at Berkeley; the discussion is, however, broadly applicable to heavy-liquid chambers as well. The size of the problem can be appreciated by considering the 5-month run now under way with the 72-inch hydrogen chamber at the Bevatron. Twenty π^- mesons passing through the chamber per expansion are expected to produce 75,000 λ hyperons, 200 λ scatterings on hydrogen, 40 leptonic decays of λs, and 3000 interesting Σ-hyperon events, plus many other interactions including

50,000 π-π interactions, plus 4,000,000 other interactions of π mesons without the production of strange particles. If analysis were at cloud chamber rates, each event would take nearly one man-day of effort. Now, with semi-automatic measuring microscopes and high-speed digital computer geometric reconstruction, the Berkeley Hydrogen Chamber Group can measure and analyze 200 events per day. Two measuring machines and a staff of 30 people are required. Systems to handle data at even higher rates have been discussed; but these multimillion-dollar systems are several years in the future.

C. Need for Accuracy

The incident particle can undergo any one of several competing reactions, which sometimes look quite similar. These must be distinguished on the basis of energy balance and momentum balance. An example is the pair of reactions

$$\text{(a)}\quad \pi^- + p \rightarrow \Sigma^0 + K^0$$

$$\text{(b)}\quad \pi^- + p \rightarrow \Lambda + K^0$$

In Case a the Σ^0 decays into a Λ plus a 70-Mev γ ray in a time $\ll 10^{-11}$ sec. In both cases, the Λ can decay to π^- + p in a mean time of 2.8×10^{-10} sec. The incoming π^- in Case a usually does not lie in the plane of the decay particles, π^- and p, since momentum is carried off by the γ ray. However, the angle of noncoplanarity (in the laboratory system) is so small that it is difficult to separate the cases, even with the most accurate measurements.

Accurate measurements are not always required. For example, information on the polarization of a beam of low-energy K^+ mesons could be obtained without any measurement, simply by counting the frequencies of scatterings to the left and to the right. Generally, however, high-energy bubble chamber experiments have required a greater accuracy of analysis than can be obtained by template measurement or graphical reconstruction.

D. Steps in Analysis

Nearly all groups have separated their data reduction and data analysis into distinct steps of searching for events, measuring the film, reconstructing the event, and tabulating it. Goldschmidt-Clermont has summarized the equipment used at various laboratories (73). More detailed description of the individual components can be found in the Proceedings of The International Meeting on Instruments for the Evaluating of Photographs, (69) held at CERN in September, 1958.

1. Scanning. The search for events is usually made on high-quality opaque projection tables. These instruments are used for initial scanning of the film, and for the check scans that are required for determining event-finding efficiency. They are also used to prepare the "sketch" instructions for the operators of the measuring machines, and are used once more to re-examine any events in which the computer output has given an anomalous result. These scanning operations take more time than the measuring operation. It is desirable, therefore, that the instruments be easy to operate, and produce good images which can be superimposed on events that need careful study. Fast and slow film transport and frame counters are desirable.

A machine for scanning film from the 72-inch Berkeley chamber is shown in Fig. 15. In this instrument any one or more of the three images can be projected onto a white micarta surface at a magnification of 10 diameters, i.e., 2/3 the original bubble chamber size. The projection lenses are Schneider Componon, 200-mm focal length, at f/5.6. It is necessary to use high-quality wide-angle lenses to keep the projection distance reasonably short. The mirrors are paralleloplate, front-surface aluminized, with a silicon monoxide coating. A special mirror suspension is required to keep the magnification sufficiently uniform throughout the picture. The three views are illuminated by three 500-watt motion picture projector lamps operating with f/0.8 Lucite condensers and Corning I-58 and I-69 heat-absorbing glasses. Film is clamped in an open-faced holder. The temperature rise of a piece of black film is no greater than 3° C.

We usually find it desirable to scan along the beam tracks, i.e., from the end of the table. It is not possible to magnify the image enough to see the necessary detail at the near end of the image without having the far end too distant from the observer. Hence the film carriage is arranged to roll easily and thereby move the image toward or away from the operator by means of a hand lever. The film can be advanced from one frame to the next in approximately 3/4 second. It can run at slew speed of 800 feet per minute, and can be started and stopped with a minimum film tension of less than 3 pounds. A frame counter automatically indicates the picture number.

2. Measuring. Special instruments have been developed by a number of laboratories for making measurements on the film to accuracies of about 2 microns. The usual instrument is a projection microscope with which the operator views the image on a translucent screen at sufficient magnification for him to position marks on the film to ± 2 micron accuracy. The film is moved to bring the point of interest on the image in coincidence with a mark fixed on the screen at the optical axis of the system. The coordinates of the stage carrying the film are measured by rotary encoders on the screws driving the stage, or by a scaler that counts fringes on gratings attached to the stage. The coordinate measurements are entered automatically on IBM cards or punched tape.

Many of the instruments are equipped with photoelectric sensing devices and tight servo loops which automatically hold the instrument centered on a track. In some instruments careful attention has been paid to designing components for high reliability, and to utilizing techniques of "human engineering" so as to minimize errors and operator fatigue.

Figure 16 shows one of the "Franckenstein MP-II" machines used for measuring film from the 72-inch bubble chamber (74). Figure 17 is a schematic diagram of the instrument. Light from a 2500-watt mercury lamp is filtered by water and heat-absorbing glass before passing through the three images on the film. These images are 1.4 by 4.9 in. After leaving the film, the light is divided by a partially silvered mirror, and passes through two lenses to give images at different magnifications. A Schneider Xenotar lens of 10.5 mm focal length produces an image at magnification of 33 on an 18-in. -square transmission screen, for making coordinate measurements. A Dallmeyer Serrac lens of 18-inch focal length projects an image of the entire chamber at a magnification of 7.5, i.e., 1/2 life size, onto an opaque screen. An illuminated reticle projected onto the half-scale view shows the region displayed on the highly magnified view. Coordinate measurements are made on the optical axis to 2.5 microns least count by using moiré fringe gratings. The sensing element for the automatic track-following screen servo is a photomultiplier mounted behind an opaque disk with 24 radial slits, spinning at 3600 rpm. The coordinates of 10 to 20 arbitrary locations on each track are recorded on perforated tape. These data are subsequently transferred to magnetic tape and put into an IBM 704 machine for computation. The cost of manufacturing one of these measuring projectors is about $140,000.

3. Computing. Most groups have divided the computation into two separate stages of geometrical and kinematic reconstruction, although their detailed philosophies in each stage may differ. In the geometrical stage each track of an event is reconstructed in space. The CERN program searches for the best helix passing close to the optical rays through the center of the

camera lens from each measured point on the stereoscopic views. (73) In the Berkeley program, developed primarily by Rosenfeld and Solmitz, a representative set of points in space is computed from the coordinates measured in the stereo views. These points are fitted to trajectories for different assumed particles, taking into account optical and magnetic-field corrections and the rate of momentum loss of the particle in hydrogen. The final fit is a fourth-order polynomial in the horizontal projection and a third-order polynomial in the vertical. The program calculates dip, azimuth, and momentum for both ends of the track, plus uncertainties and correlation coefficients between all the output quantities. The Berkeley programs are described in several physics notes, and are summarized in Rosenfeld's paper at the 1959 CERN conference. (75)

For the kinematical stage, the most powerful and versatile program has been developed by Rosenfeld and his associates. It was summarized at the 1959 CERN Symposium, and is described in a series of articles by Rosenfeld, Solmitz, Snyder, Taft, and others (76). The equations of energy balance and momentum balance impose constraints on the interrelations between the momentum components of the observed tracks. The program calculates the constrained momentum components which approximate the measured values, and prints out the relative goodness of fit for the different possible interpretations together with all fitted information specified by the physicist.

The time required for the complete computation in the IBM 704 is approximately 1 minute, representing a computing cost of about \$1 per event. This is to be compared with a total cost of operating the Bevatron and bubble chamber of approximately \$3 per pulse. Interesting events occur as often as one per pulse, or as rarely as one per 10,000 pulses, depending on the experiment.

The output from the computing machine must be examined and tabulated, or remeasured if an error is evident. The task of bookkeeping is getting increasingly large and will require complicated computer programs. Apparently the most sophisticated effort in this direction up to the present has been made by White, in connection with analysis of propane bubble chamber film at Berkeley (77).

The steps in the analysis operation and the required times are summarized in Table IV.

VIII. SUPPLEMENTARY DATA FOR EXPERIMENTERS

This section presents a compilation of data to aid physicists in planning experiments. The data are not intended to be a basis for precise computation. The limits of their applicability are not discussed at length, and assumptions made in the development of equations are not detailed. The reader should refer to the cited literature for more details.

A. Comparison of Bubble Chamber Liquids

Table V shows comparative characteristics of a number of bubble chamber liquids. Density and radiation length are taken from table I. Values of dE/dx at minimum for H_2 and propane are taken from Barkas and Rosenfeld (78). The value for propane was changed by a factor of 44/41, to compensate for the different density used. Other values of dE/dx, and stopping power, were obtained from the high energy particle data of Atkinson and Willis (79). Values for $SnCl_4$ and CF_3Br were assumed to be the linear sums of the values for the atomic constituents of the compounds. Scattering sagitta and required magnetic field are computed from the formulas in section B, below. The number of events per day is based on present average running conditions of 30 tracks per expansion, and 6,000 expansions per day.

The following barn-door conversions are useful for order-of-magnitude planning with the 72-inch hydrogen bubble chamber:

1 barn per foot of track,

1 millibarn per minute of running,

1 microbarn per day of running

Thus, π-p scatters with 30 mb cross section occur at the rate of 30 per minute.

B. Multiple Coulomb Scattering Formulae

The accuracy with which momentum can be obtained by measuring track curvature in a magnetic field is limited by multiple Coulomb scattering of the charged particles. A convenient expression for the root mean square curvature due to multiple Coulomb scattering is

$K_{sc} = \sqrt{2/3}\ (21/p\beta)/\sqrt{LX}\ \mathrm{cm}^{-1}$, where p = momentum in Mev/c, β = velocity divided by velocity of light, L = length of track, X = radiation length.

The root mean square value of the sagitta, δ, due to multiple Coulomb scattering curvature is given by $\delta = \dfrac{2.14\ L^{3/2}}{p\beta\ X^{1/2}}$ cm.

The curvature of a singly charged particle of momentum p in a magnetic field of H kilogauss is

$$K_H = 0.3\ H/p\ \mathrm{cm}^{-1},$$

hence the fractional uncertainty in momentum is

$$K_{sc}/K_H = \sqrt{\frac{2}{3}}\ \frac{21}{0.3\ \beta H}\ \sqrt{\frac{1}{LX}}\ .$$

For the particular case of a hydrogen bubble chamber this reduces to

$$K_{sc}/K_H \doteq 1.2/(\beta H\sqrt{L}) \text{ for hydrogen.}$$

More accurate values of multiple Coulomb scattering are given by Barkas and Rosenfeld (78). Kim (80) has given a more complete treatment of the momentum accuracy obtainable under the combined influence of the magnetic field and multiple Coulomb scattering. Williams (29) discusses this point, and also considers the uncertainty of angle measurements under the combined influence of multiple Coulomb scattering and measurement errors.

C. Delta Rays

The collision of an energetic particle with a stationary electron ejects the electron at an angle and energy dependent only on the center of mass velocity of the incident particle. Crawford (81) describes a method of obtaining the mass by measuring angle and energy of δ rays from an incident particle whose momentum is known. There is, of course, a lower limit to the length of δ ray for which satisfactory measurements can be made. Figure 18 shows the cross section and mean free path in liquid hydrogen for producing δ rays, 5 mm long and 10 mm long, by particles of various incident momentum $\div$ mass. The length of a delta ray can sometimes permit a mass determination without measurement of angles, since the maximum possible δ-ray energy is a function of both the momentum of the particle and its mass. Figure 19 shows the regions of momenta in which δ-ray measurements and gap counts are useful for distinguishing various particles in liquid hydrogen. Shaded regions at the bottom of each section show the momenta for which different methods are applicable. Protons, for example, stop in a 20-inch chamber if their momentum is less than about 0.3 Bev/c. If we assume that gap counting is satisfactory for ionization of 0.9 I_{min}, we conclude that gap counting is useful for proton momentum up to about 3 Bev/c. At higher momentum the ionization is too close to minimum. At the other end of the scale, the probability of having a δ ray long enough to measure is too small for proton momentum less than about 1 Bev/c. The appearance of a δ ray longer than 10 cm on a 1.5-Bev/c track would immediately rule out the possibility that the particle is a proton.

D. Polarization

Figure 20 shows the polarization in proton-proton scattering for various laboratory-system angles and laboratory-system momenta. (82) Figure 21 presents similar data for proton polarization from elastic scattering in carbon (82). Points lying above the dashed line are in a region in which elastic processes can be confused with inelastic ones. Observations in this region might be unreliable. Figure 22, compiled from data of Gammel & Thaler, shows proton polarization in proton-helium scattering (83).

E. Range-Energy and Range-Momentum Relations

Figure 24 shows range as a function of energy for various particles in hydrogen bubble chambers (84), and in propane chambers (85). Figure 25 gives range as a function of momentum for the same particles. The data for hydrogen and propane are plotted on the same graph, to make comparison easy. The curves are valid to the accuracy that can be read from these graphs, but the literature references should be consulted for more precise data.

F. Effort Required in an Experiment

The following information was compiled at the end of the recent antiproton run at the Bevatron with the 72-inch hydrogen bubble chamber (86).

The experiment ran for a period of 17 weeks in July - October, 1959. The manpower used, exclusive of Bevatron operation and maintenance, averaged over the whole period of the run, was as follows:

Technicians	Total Man-Hours	Full-Time Equivalent
Bubble chamber crew (4 per shift + compressor room and supervision)	18,400	27
Support for bubble chamber	7,900	13
Photographic	3,400	5
Data-reduction maintenance	2,040	3
Scientific Assistants		
Beam watching	2,880	4-1/4
Scanning and Measuring	4,640	6-3/4
Converting tapes, running programs, etc.	620	1
	40,800	60
Physicists (Ph. D. s and Graduate Students)		
3 per shift		13

Five physicists worked on the experiment during the whole run, and about eight others worked on it for some period of the run. There should probably be about twice as many physicists assigned to an experiment of this complexity.

During this time 255 rolls of film were exposed, each containing about 600 stereo triads. The chamber was operated 24 hours a day, at a repetition rate of about 3 per minute. Under these conditions the Bevatron is capable of about 10^5 pulses per week; the chamber was able to accept about 3×10^4 pulses per week. About 10^4 pictures per week were taken. This 1/3 efficiency is a measure of the difficulty of keeping such complicated equipment running, since the Bevatron beam spectrometers and bubble chamber ran "pretty well."

Physics with large bubble chambers has indeed become a big effort. It can be expected to become bigger as scientists develop ways to handle a larger proportion of the interesting events that exist in bubble chamber pictures. However, there is not yet any other tool that combines the important characteristics of hydrogen bubble chambers for high-energy nuclear physics investigations. The trends with other existing types of detectors, such as counters, are toward large counter arrays and digital-computer data processing that are comparable in cost and complexity to bubble chamber operations.

This work was done under the auspices of the U. S. Atomic Energy Commission.

LITERATURE CITED

1. Fretter, W. B., Annual Review of Nuclear Science, 5, 145-78 (1955).
2. Ogden, B. K., CERN Bibl 2 (1958)
3. Amiot, P. and Ogden, B. K., CERN Bibl 3 (1959)
4. Glaser, D. A., Phys. Rev., 87, 665 (1952)
5. Glaser, D. A., Phys. Rev., 91, 762-63 (1953)
6. Glaser, D. A. and Rahm, D. C., Phys. Rev., 97, 474-79 (1955).
7. Wood, J. G. Phys. Rev., 94, 731 (1954).
8. Glaser, D. A., Handbuch der Physik, 45 (Springer, Berlin, 1958) p 314-341
9. Bradner, H. and Glaser, D. A., Second International Conference on the Peaceful Uses of Atomic Energy, Vol 14, paper P/730 (United Nations, Geneva, 1958), p. 412-22
10. Glaser, D. A., Nuovo cimento, 11, Suppl 2, 361-68 (1954)
11. Seitz, F., Phys. of Fluids, 1, 2-13 (1958)
12. Glaser, D. A., Rahm, D. C., and Dodd, C., Phys. Rev., 102, 1653-58 (1956)
13. Willis, W. J., Fowler, E. C., and Rahm, D. C. Phys. Rev., 108, 1046-47 (1957)
14. Blinov, G. A., Krestnikov, Iu. S., and Lomanov, M. F., Zhur. Eksptl. i Teoret Fiz., 31, 762-70 (1956) (in Russian)
    Soviet Phys JETP, 4, 661-70 (1957) (in English).
15. Bassi, P., Loria, A., Meyer, J. A., Mittner, P. and Scotoni, I., CERN Symposium on High Energy Accelerators and Pion Physics, 1956 vol 2. p 28
16. Birss, I. R., Nature 184 Suppl. 19, 1474 (Nov. 7, 1959)
17. Plessett, M. S., and Zwick, S. A., J. Appl. Phys., 25, 493-500 (1954)
18. Birkhoff, G., Margulies, R. S., and Horning, W. A., Phys. of Fluids, 1, 201-04 (1958)

19. Bassi, P., Loria, A., Meyer, J. A., Mittner, P., and Scotoni, I., Nuovo cimento, 4, 491-500 (1956)

20. Bugg, D. V., Progress in Nuclear Physics, Vol 7 (Pergamon Press, London, New York, Paris, Los Angeles, 1959), p 1-52.

21. Rossi, B., High Energy Particles (Prentice-Hall Inc., New York 1952) p 220.

22. See, for example,

Alvarez, L. W., Fifth Rochester Conference on High Energy Nuclear Physics (Interscience Publishers, New York, 1955), Chapter VII, p 181-82.

Alvarez, L. W., Second International Conference on Peaceful Uses of Atomic Energy, Vol 30, paper p/729 (United Nations, Geneva, 1958) p 164-65.

Eisler, F., Plano, R., Prodell, A., Samios, N., Schwartz, M., Steinberger, J., Bassi, P., Borelli, V., Puppi, G., Tanaka, H., Waloschek, P., Zobeli, V., Conversi, M., Franzini, P., Manelli, I., Santangelo, R., and Silvestrini, V., Nuovo Cimento 10, 468-489 (1958)

Gow, J. D., Second International Conference on Peaceful Uses of Atomic Energy, Vol 30, paper p/733 (United Nations, Geneva, 1958), p 166-73.

Various authors - International Conference on High Energy Accelerators and Instrumentation, (CERN, 1959), p 435-60.

23. See, for example

Block, M. M., Fairbank, W. M., Harth, E. M., Kikuchi, T., Meltzer, C., and Leitner, J., International Conference on High Energy Accelerators and Instrumentation (CERN, 1959), p 461-65

See also references 130-135 of CERN Bibl. 2, cited as reference 2 in this review paper.

24. See, for example

Bloch, M., Lagarrigue, A., Musset, P., Rancon, P., Rousset, A., Sauteron, X., and Six, J., International Conference on High Energy Accelerators and Instrumentation, (CERN 1959), p 499-502.

See also references 146-163 of CERN Bibl 2, cited as reference 2 in this review paper.

25. Kamarek, T. I., Maltsev, E. I., Nagy, T., Nagy, J., Prokes, A., Stashkov, G. M., Ustenko, E. P., Chuvilo, I. V., and Skhobin, U. N., International Conference on High Energy Accelerators and Instrumentation (CERN, 1959), p. 506-08.

26. Brown, J. L., Bryant, H. C., Burnstein, R. A., Hartung, R. W., Glaser, D. A., Kadyk, J. A., Sinclair, D., Trilling, G. H., VanderVelde, J. C., and van Putten, J. D., Phys. Rev. Letters, 3, 51 (1959)

27. Alyea, E. D., Gallagher, L. R., Mullins, J. H., and Teem, J. M., Nuovo cimento, 6, 1480-88 (1957)

28. Bugg, D. V., Rev. Sci. Instruments, 29, 587-89 (1958)

29. Williams, R. W. Canad. J. Physics, 37, 1085-99 (1959).

30. Hildebrand, R. H. (University of Chicago, Enrico Fermi Institute), private communication.

31. See references 115-129 of CERN Bibl. 2, cited as reference 2 in this review paper.

32. Bertranza, L., Martelli, G., and Zacutti, A., Nuovo cimento, 2, 487-94 (1955).

33. Hahn, B., Riepe, G., and Knudsen, A. W., Rev. Sci. Instruments, 30, 654-55 (1959)

34. Kalmus, G. E., Meeting on Heavy Liquid Bubble Chambers, CERN 59-24 (CERN, Geneva, July 1959) p 33-39.

35. Hahn, B., Meeting on Heavy Liquid Bubble Chambers, CERN 59-24 (CERN, Geneva, July 1959) p 39-55.

36. Alichanyan, A. I., Veremeev, M. M., Galper, A. M., Kirillov-Ugrumov, W. G., Kotenko, L. P., Kusin, L. A., Kuznetsov, E. P. and Popov, U. S., International Conference on High Energy Accelerators and Instrumentation (CERN 1959) p 512-14.

37. Resegotti, L., CERN 59-24 (CERN, Geneva, July 1959) p 31-32.

38. Pless, I., (Massachusetts Institute Technology), private communication.

39. Henderson, C., CERN 59-24, (Geneva, July 1959) p 26-30.

40. Rousset, A., CERN 59-24 (Geneva, July 1959) p 17-24, and International Conference on High Energy Accelerators and Instrumentation, (CERN 1959) p 499-503.

41. Plano, R. (Columbia University) private communication.

42. Powell, W. M., (Lawrence Radiation Laboratory, Berkeley) private communication.

43. Barford, N. C., Progress in Cryogenics, Vol 2 (Heywood, London, 1960)

44. Rahm, D. C., International Conference on High Energy Accelerators and Instrumentation, (CERN 1959), p 440-41.

45. Gow, J. D., and Rosenfeld, A. H., International Conference on High Energy Accelerators and Instrumentation, (CERN 1959), p 435-39

46. Franck, J. V., University of California Radiation Laboratory Report UCID-71, March 1956.

47. Riddiford, L., Van de Raay, H. B., Barford, N. C., Butler, C. C., McMullan, D., Thetford, A., Thomas, D. B., Welford, W. T., Amery, A., Evans, W. H., Moore, M. J., Polak, P., Skinner, H. W. B., Williams, P. R., Shaw, D., Ashburn, A. G. and Snowden, M., International Conference on High Energy Accelerators and Instrumentation, (CERN 1959) p 445-53.

48. Peyrou, Ch., International Conference on High Energy Accelerators and Instrumentation, (CERN 1959), p 454-59.

49. Belonogov, A. V., Zeldovich, A. G., Kolganov, V. Z., Landsberg, L. G., Lebedev, A. V., Nikitin, S. Ia., Smoliankin, V. I., Sokolev, A. P., Pribory i tekh. eksper. 1958 No. 1, p 38-41 (Russian) or AEC translation 3664.

50. Nikitin, S. Ia. (U. S. S. R.), private communication.

51. Eaton, W., and Hernandez, H. P., University of California Radiation Laboratory Report, UCRL-8134, Oct. 1955.

52. Kropschot, R. H., and Mikesell, R. P., National Bureau of Standards Report 3590, June 22, 1956.

53. Amiot, P., Nullens, G., and Spondlin, R., CERN 59-20 (CERN, Geneva, 1959)

54. Peyrou, Ch. (CERN), private communication.

55. Ross, R., University of California Radiation Laboratory Report, UCID-146, May 1958.

56. See, for example, Davies, G. E., J. Optical Soc. Am., 45, 572 (1955)

57. Nagel, D. E., Hildebrand, R. H., and Plano, R. J., Rev. Sci. Instruments, 27, 203-07 (1956)

58. Bradner, H., (Lawrence Radiation Laboratory, Berkeley) unpublished work.

59. Alvarez, L. W., University of California Lawrence Radiation Laboratory Report, UCID-977, April 1960.

60. Rosenfeld, A. H. and Solmitz, F. T., University of California Radiation Laboratory Report, UCID-186, May 1958.

61. Schwemin, A. J., (Lawrence Radiation Laboratory, Berkeley), private communication.

62. Wilson, J. G., Principles of Cloud Chamber Techniques (Cambridge University Press, London 1951).

63. Good, M. L., University of California Radiation Laboratory Report, UCID-29, April 1955

64. Bradner, H., (Lawrence Radiation Laboratory, Berkeley), unpublished work.

65. Welford, W. T., (Imperial College, London), unpublished work.

66. Kuznetsov, E. V., Lomanov, M. F., Blinov, G. A., Chuan Chen-Niang, and Khwan Shen-Nian, Zhur Eksptl i Teoret Fiz., 31, 911 (1956) (Russian), and Soviet Phys-JETP 4, 773-74 (1957) (English)

67. Donaldson, R. and Watt, R., University of California Radiation Laboratory Report, UCID-117, Feb. 1956.

68. CERN Symposium on High Energy Accelerators and Pion Physics, 1956, Vol. 2.

69. International Meeting on Instruments for Evaluation of Photographs, CERN 58-24 (1958).

70. International Conference on High Energy Accelerators and Instrumentation CERN 1959

71. Bradner, H. and Solmitz, F., Second International Conference on the Peaceful Uses of Atomic Energy Vol. 14, Paper P/2515 (United Nations, Geneva, 1958) p 423-26

72. Bradner, H., University of California Lawrence Radiation Laboratory Report, UCRL-9104, Jan. 1960

73. Goldschmidt-Clermont, Y., International Conference on High Energy Accelerators and Instrumentation, (CERN 1959), p 523-32

74. Franck, J. F., et al., Review of Scientific Instruments, to be published.

75. Rosenfeld, A. H., International Conference on High Energy Accelerators and Instrumentation (CERN 1959), p 533-41

76. Rosenfeld, A. H. and others, to be submitted to Rev. Sci. Instruments.

77. White, H., University of California Lawrence Radiation Laboratory Report, to be published.

78. Barkas, W. H. and Rosenfeld, A. H., Data for Elementary-Particle Physics, University of California Radiation Laboratory Report, UCRL-8030, March 1958.

79. Atkinson, J. H. and Willis, B. H., University of California Radiation Laboratory Report, UCRL-2426 rev. Vol II, June 1957

80. Kim, Y. B., Rev. Sci. Instruments, 29, 680-88 (1958).

81. Crawford, F. S., University of California Radiation Laboratory Report, UCID-241, Nov. 1957.

82. Birge, R. W. (Lawrence Radiation Laboratory, Berkeley), unpublished work.

83. Gammel, J. L. and Thaler, R. M., Phys. Rev., 109, 2041-47 (1958).

84. Rosenfeld, A. H., University of California Radiation Laboratory Engineering Note, 4310-03-M6, Feb. 1956.

85. Birge, R. W., University of California Lawrence Radiation Laboratory Report, UCID-1052, Sept., 1959

86. Alston, M. and Blumberg, R., University of California Lawrence Radiation Laboratory Report, UCID-1054, Nov. 1959.

[1] The survey of literature pertaining to this review was completed in April, 1960.

[2]Radiation length, L_{rad}, is calculated from equation (1) in Rossi, "High Energy Particles", p. 220 (21). L_{rad} is a measure of the accuracy that can be obtained in momentum determinations, since multiple Coulomb scattering produces an uncertainty in track position proportional to $(L_{rad})^{-1/2}$. Also it is a measure of the efficiency that can be expected in pair production by gamma rays, since the mean conversion distance is proportional to L_{rad}.

TABLE I

OPERATING PARAMETERS OF BUBBLE CHAMBERS

Liquid	Temp	Pressure, absolute (atm)	Expansion (%)	Density	Radiation length (cm)	Flash delay (msec)	Index refraction 5300 A°	Source of data
H_2	28±2 °K	~ 5.3	~ 2-4	0.0586	≈ 1100	~ 2	1.093	Alvarez Shutt
D_2	32±2 °K	~ 7.3	~ 2-4	~0.13	~ 950	~ 2	~1.1	Alvarez
He	~ 3.4 °K	~ 1	$\lesssim$ 1	~0.124	~ 900	~ 5	~1.03	Block(23)
Propane (C_3H_8)	58 °C	~ 21	~ 3	~0.44	~ 110	~ 1	~1.22	Powell
CF_3Br	28±4°C	~ 18	~ 3	~1.5	~ 11	~ 3	--	Bugg (28) Kalmus (34)
Xenon	-19 °C	~ 25	~ 3	~2.18	~ 8.6	~ 3	~1.18	Glaser

TABLE II

LARGE HEAVY LIQUID (FREON OR PROPANE) CHAMBERS COMPLETED OR UNDER CONSTRUCTION

Name	Size	Magnet	Windows	Reference
Alichanyan-Lebedev, Moscow	90 cm deep; 90 cm. diam. 570 liters	none	one	(36)
CERN, Geneva[a]	50 cm deep; 100 cm. diam. 500 liters	⩾ 18 kgauss 4.5 Mw	one	(37)
Mass. Inst. Tech.[a]	15 in. deep; 40 in. diam. 310 liters	15 kgauss	one	(38)
Dodd-Univ. College,[a] London	40 cm. deep; 50 × 140 cm 300 liters	~ 15 kgauss 4 Mw		(39)
Lagarrigue-Ecole Polytechnique Paris	50 cm. deep; 50 × 100 cm 300 liters	20 kgauss 4.5 Mw	three	(40)
Steinberger-Brookhaven	14 in. deep; 30 in. diam. 160 liters	15 kgauss	one	(41)
Powell-Lawrence Lab., Berkeley	6.5 in. deep; 18 × 30 in. 57 liters		one	(42)

[a]Data are tentative.

TABLE III

TENTATIVE PARAMETERS OF SOME LARGE HYDROGEN BUBBLE CHAMBERS AND THEIR MAGNETS

Chambers	Dimension of illuminated volume (inches)	Volume of hydrogen (liters)	Material	Number of windows	Window location	Expansion mechanism
Berkeley	14×20×72	520	Cast stainless steel	1	Top	Vapor
Brookhaven	28×25×80	1700		1	Side	Liquid (piston)
British Nat'l	18×20×59	~500	Machined aluminum	2	Side	Vapor
CERN	20×24×78	~1000	Cast or welded stainless steel	2	Side	Liquid (piston)

Magnet	Field (kgauss)	Power (Mw)	Field homo-geneity	Pole pieces	Weight of Cu (tons)	Weight of Fe (tons)	Total wt. (tons)	Cost $\$ \times 10^3$
Berkeley	18	2.5	± 12%	1	20	115	~200	200
Brookhaven	~17	4	"few %"	1	30	250	280	——
British Nat'l	11.8	4	"few %"	0	40.2	240	300	——
CERN	~16.6	6	——	0	——	——	470	——

TABLE IV

OPERATION IN DATA PROCESSING

OPERATION	EQUIPMENT	OUTPUT	COMMENTS and	APPROXIMATE TIME/EVENT
Run Experiment	Bubble Chamber	Film	Typical reactions, e.g. $\pi^- + p \rightarrow \Lambda + K^0$ may occur once every	5 min.
Scan	Scan Table	Handwritten Scan Form	Physicist or skilled assistant searches for interesting reactions............................	Typical 10 min.
Sketch	Scan Table	Sketch card	Physicist designates event type, numbers tracks, and specifies which views to be measured...........	5 min.
Measure	Franckenstein	Track Co-ordinates (15-inch: IBM cards) (72-inch: Paper Tape)	(1) Technician advances film, sets in fixed data, measures fiducials, etc......................	5 min.
			(2) Then he measures about 10 xy-coordinates on two views of each track.	5 min.
Card-to-Tape or Tape-to-Tape	IBM Card-to-Tape or our own tape-to-tape			

IBM PROGRAM	EQUIPMENT	OUTPUT	COMMENTS and	APPROXIMATE TIME/EVENT
PANG (P and ANGle)	IBM 704	Track $\vec{p}, \delta\vec{p}$, etc.((*) Print-outs + Binary Tape)	(1) Computes space-synthesis of points and makes zero-order fit........................	2/3 sec/track
			(2) Makes one final fit for each mass assignment.	1/2 sec/track
KICK K-Interaction Coplanarization and Kinematics	IBM 704	X^2 + fitted data with errors((*) Binary Tape)	(1) Computes Kinematic fit of each vertex to assigned hypotheses..........................	3 seconds
			(2) Combines successful vertex fits into multi-vertex events................................	3 sec. x number of vertex fits.
EXAMIN (and print KICK output	IBM 704	(*) Printouts	Prints, selects event with special criteria, makes histograms, keeps books.....................	3 sec. to write a vertex fit
			TOTAL 704 time for average event...................	1/2 min.
DRIVEL	IBM 704	(*) Magnetic Tape	Merges and sorts KICK-format tape.	

(*) Except for lists of mistakes, printed by the on-line printer, all our data come out of the 704 on magnetic tape; binary tape if the output is to be used as input for later programs, plus additional BCD (Binary Coded Decimal) tape to feed to our off-line printer if desired.

TABLE V

COMPARISON OF VARIOUS BUBBLE CHAMBER LIQUIDS

LIQUID	DENSITY	RADIATION LENGTH	dE/dx AT MINIMUM	SCATTERING SAGITTA FOR 2 BEV/c TRACK 20 cm LONG	MAGNETIC FIELD REQUIRED FOR 5 % MOMENTUM UNCERTAINTY IN 20 cm RELATIVISTIC TRACK	STOPPING POWER OF 50 cm CHAMBER	EVENTS PER DAY IN 50 cm CHAMBER AT σ PER NUCLEON=1μ BARN	COLLISION MEAN FREE PATH FOR σ = 10mb/ nucleon	COLLISION mfp in HYDROGEN FOR σ = 10 mb/hydrogen nucleus
	(gm/cm^3)	(cm)	(Mev/c)	(microns)	(Kg.)	(gm/cm^2)		(cm)	(cm)
H_2	0.059	1100	0.24	20	8	2.5	0.27	2800	2800
D_2	0.13	950	0.22	22	8.5	2.6	0.28	1270	-
He	0.124	900	0.21	23	8.7	5.0	0.54	1330	-
Propane (C_3H_3)	0.44	110	1.0	65	25	22	2.3	370	2040
$Sn\ Cl_4$	1.5	8.6	2.2	230	90	75	8	110	-
CF_3Br	1.5	11	2.5	200	80	80	8	110	-
Xenon	2.18	3.7	2.8	350	135	110	11	76	-

Figure Captions

Fig. 1. Pressure-volume plot of representative isothermal curves for a real gas.

Fig. 2. Twelve-inch-diameter propane chamber. (Courtesy Prof. R. J. Plano)

Fig. 3. Schematic assembly drawing of 12-inch-diameter propane chamber (Courtesy Prof. R. J. Plano)

Fig. 4. Normal range of operating temperature and pressure for hydrogen bubble chambers. (Courtesy of H. B. Barford)

Fig. 5. Twenty-inch hydrogen bubble chamber. (Courtesy Dr. Ralph Shutt)

Fig. 6. Model showing cutaway view of 72-inch hydrogen bubble chamber.

Fig. 7. Longitudinal cross section of 72-inch hydrogen bubble chamber.

Fig. 8. Photograph of 72-inch hydrogen bubble chamber and hydrogen shield.

Fig. 9. Schematic cross section of inflatable gasket.

Fig. 10. Retrodirective illumination of 72-inch hydrogen bubble chamber.

Fig. 11. Plan view of 18 × 20 × 59-inch. British National hydrogen bubble chamber (schematically, Riddiford et al (47)

Fig. 12. Transverse cross-section of 28 × 25 × 80-inch Brookhaven hydrogen bubble chamber. (Courtesy Dr. Ralph Shutt)

Fig. 13. Magnetic field strength in the 72-inch hydrogen bubble chamber as a function of ampere turns for different weights of iron in the return path.

Fig. 14. Intensity of light scattered at angle θ for gas bubbles in liquids with different values of index of efraction. (Courtesy H.B. Barford)

Fig. 15. Schematic view of "Coat hangers" for retrodirective illumination.

Fig. 16. Formation of bubble image by camera lens.

Fig. 17. "Scanning projector" for examining film from 72-inch hydrogen bubble chamber.

Fig. 18. "Franckenstein" measuring projector for film from 72-inch hydrogen bubble chamber.

Fig. 19. Schematic drawing of "Franckenstein" measuring projector for film from the 72-inch hydrogen bubble chamber.

Fig. 20. Cross section and mean free path in liquid hydrogen chamber for producing δ rays of greater range than R_{min}, vs $\beta\gamma$, for three different values of minimum range.

Fig. 21. Values of momentum for which particle identification can be made by δ rays, by gap counting, or by range.

Fig. 22. Polarization in proton-proton scattering. Contours are labeled by polarization in percent.

Fig. 23. Polarization of protons elastically scattered from carbon. Contours are labeled by polarization in percent.

Fig. 24 Polarization of protons scattered from helium. Contours are labeled by polarization in percent.

Fig. 25. Energy vs. range in hydrogen bubble chamber and in propane bubble chamber.

Fig. 26. Momentum vs. range in hydrogen bubble chamber and in propane bubble chamber.

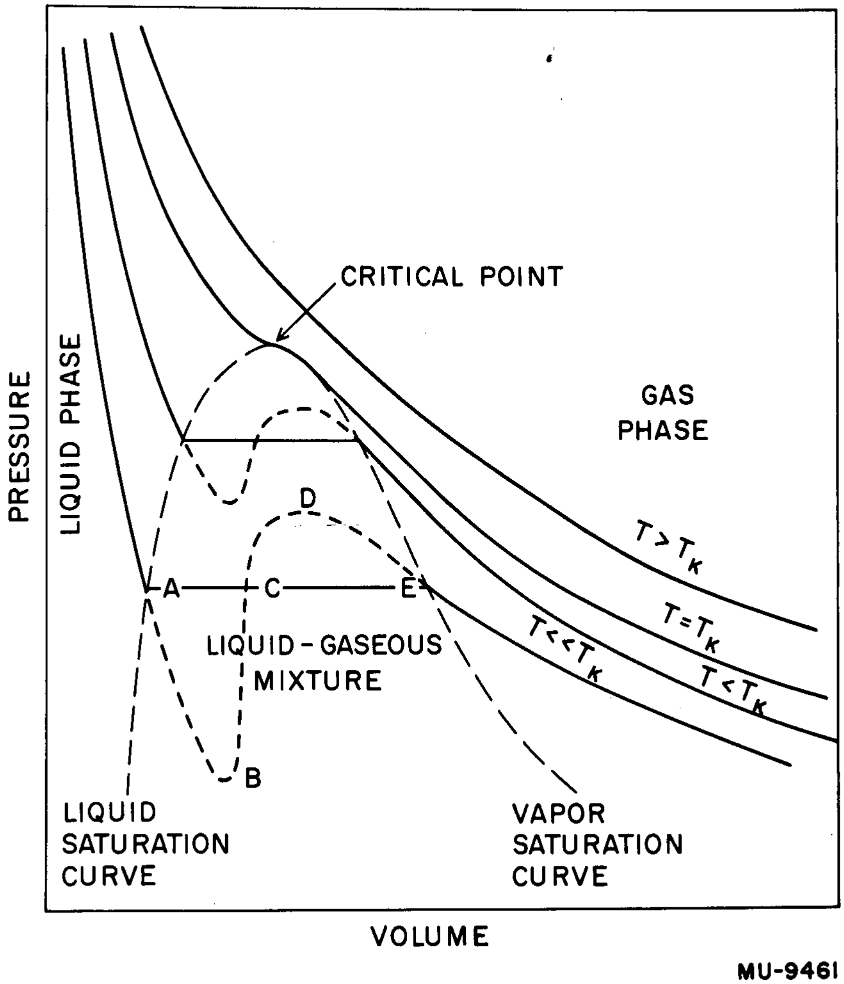
CRITICAL POINT
GAS PHASE
PRESSURE
LIQUID PHASE
D
A
C
E
B
LIQUID-GASEOUS MIXTURE
T > T_K
T = T_K
T << T_K
T < T_K
LIQUID SATURATION CURVE
VAPOR SATURATION CURVE
VOLUME
MU-9461

Fig. 1

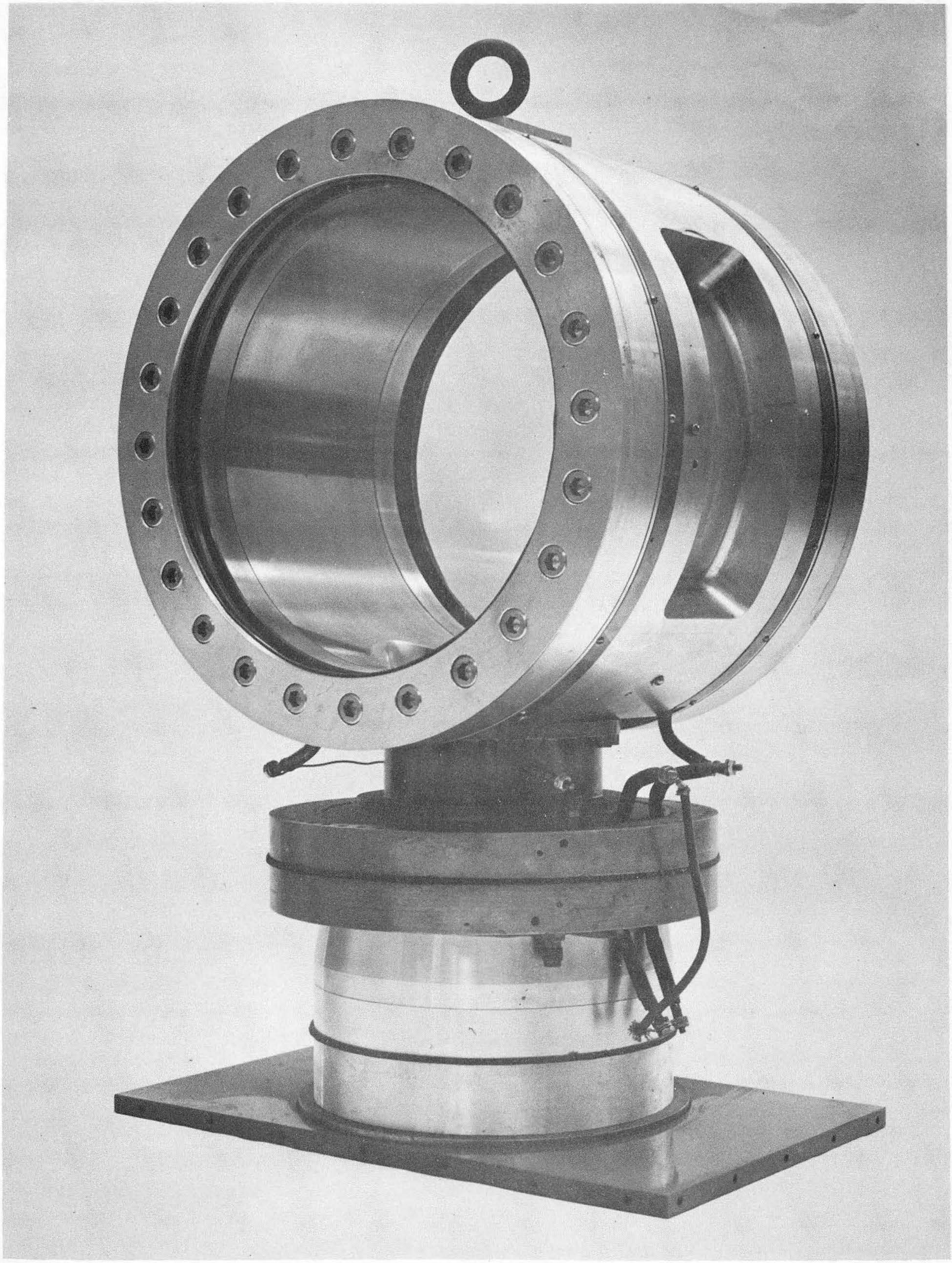

ZN-2457

Fig. 2

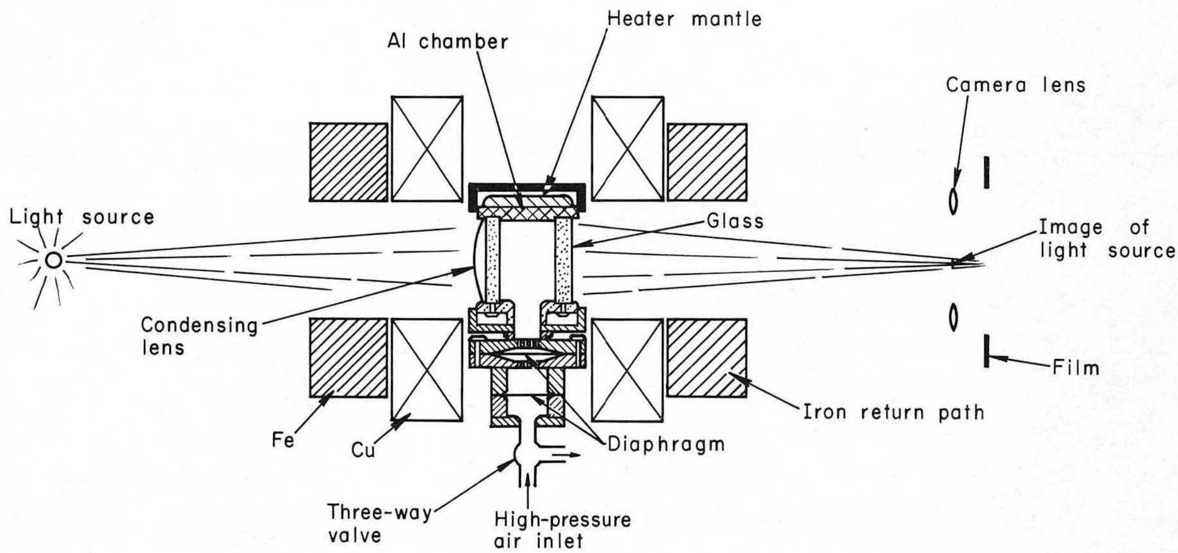

Heater mantle
Al chamber
Camera lens
Light source
Glass
Image of light source
Condensing lens
Film
Iron return path
Fe
Cu
Diaphragm
Three-way valve
High-pressure air inlet
MU-20238

Fig. 3

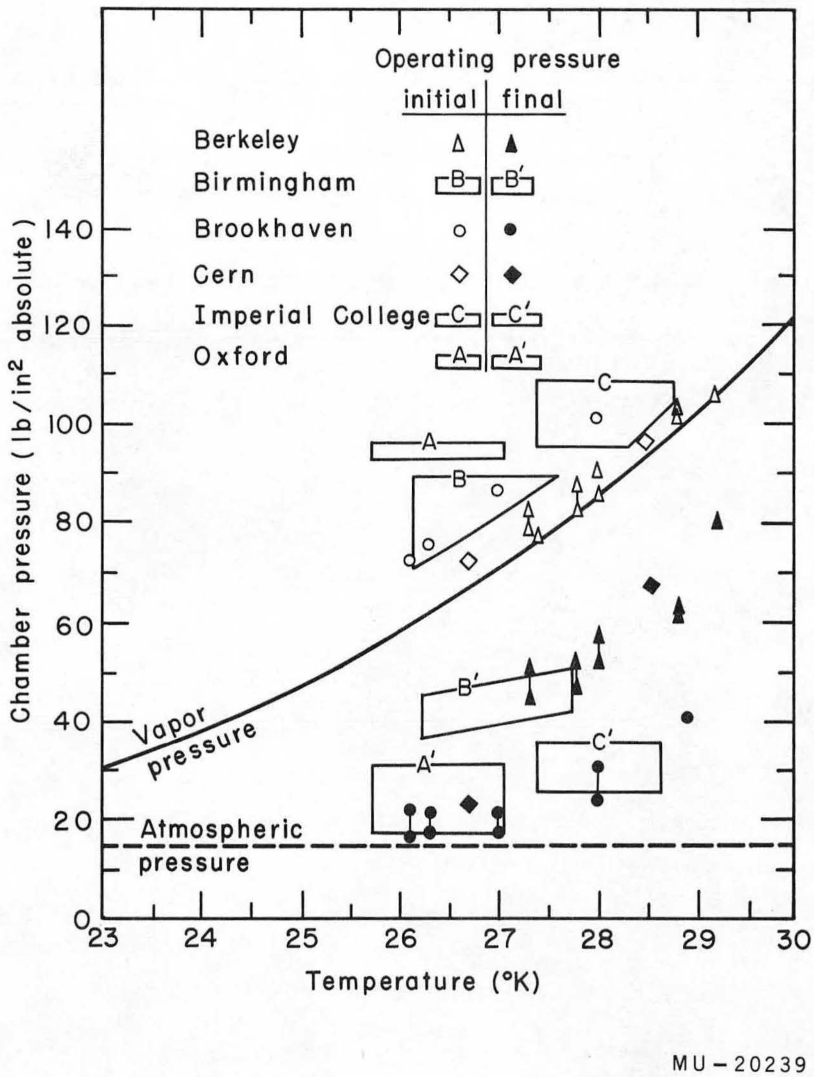
Operating pressure
initial
final
Berkeley
Birmingham
Brookhaven
Cern
Imperial College
Oxford
Chamber pressure (lb/in² absolute)
Temperature (°K)
Vapor pressure
Atmospheric pressure
A
B
C
A′
B′
C′
0
20
40
60
80
100
120
140
23
24
25
26
27
28
29
30
MU-20239

Fig. 4

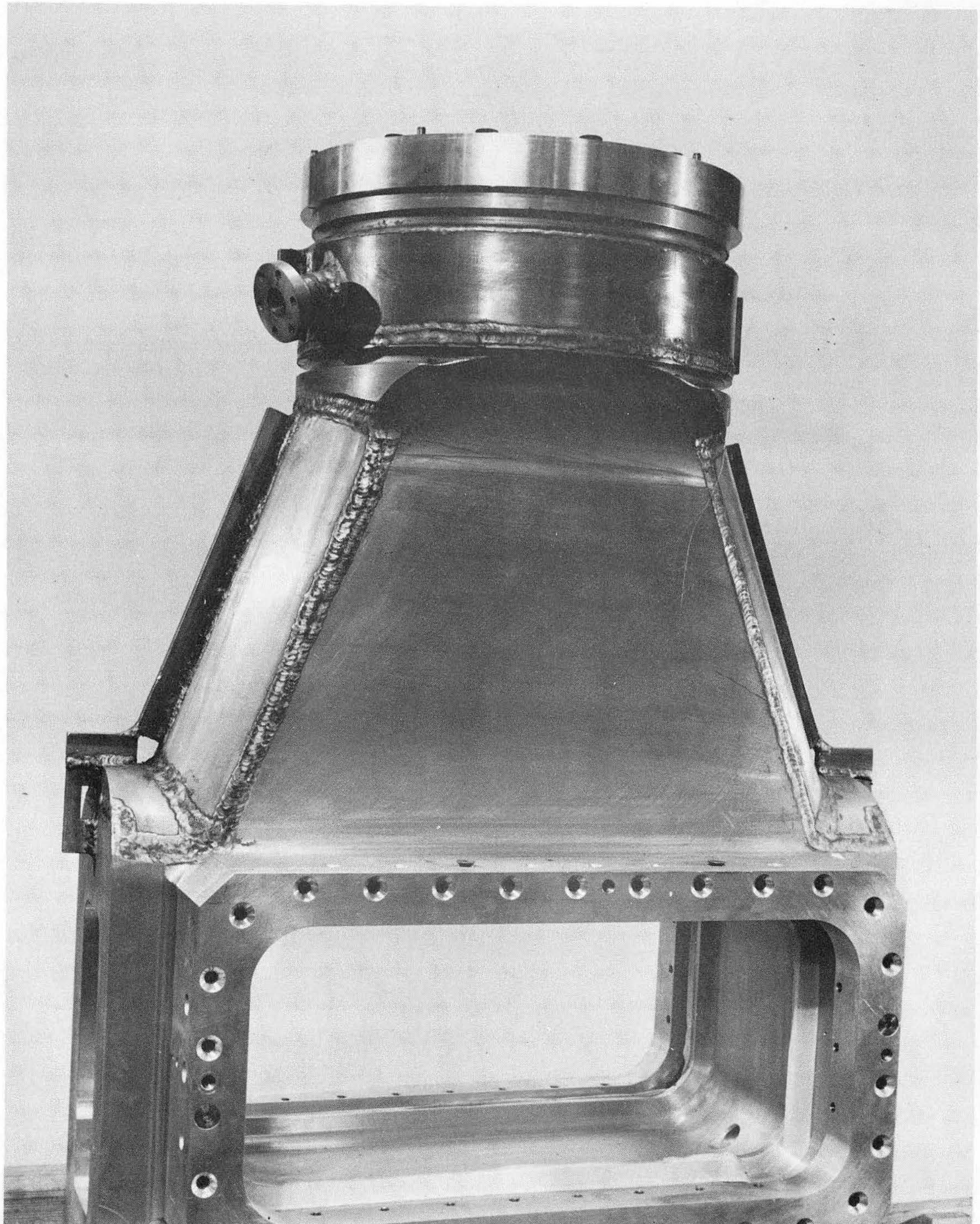

ZN-2458

Fig. 5

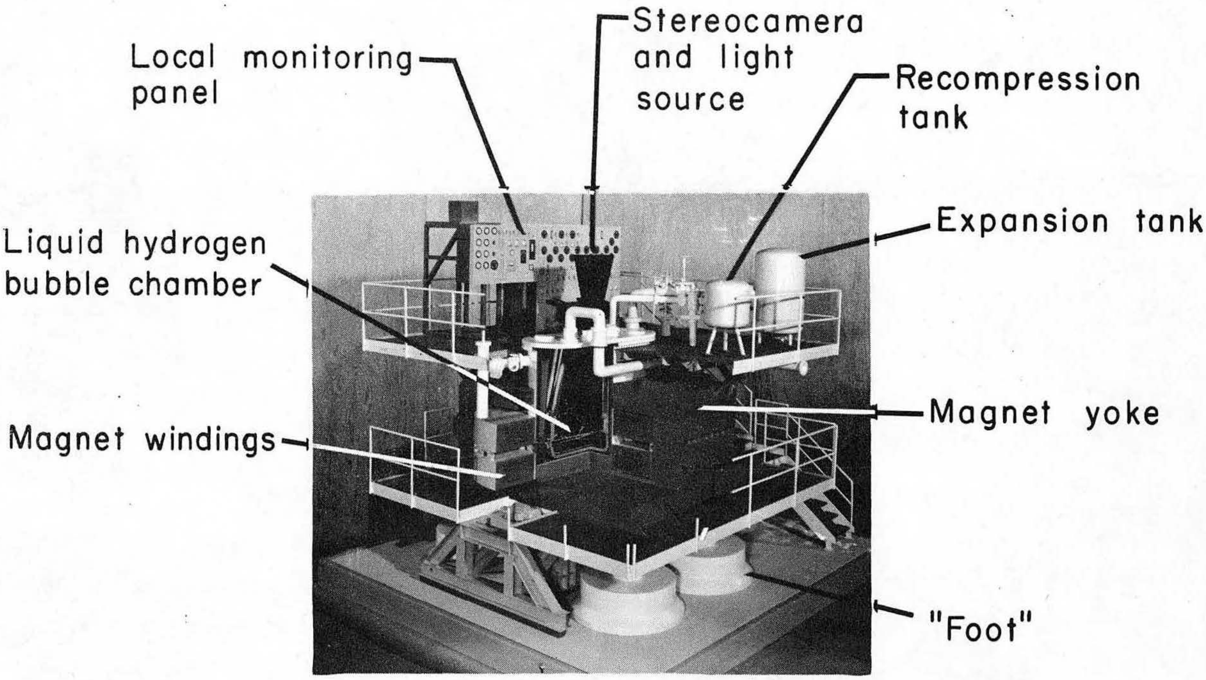
Local monitoring panel
Stereocamera and light source
Recompression tank
Expansion tank
Liquid hydrogen bubble chamber
Magnet yoke
Magnet windings
"Foot"

ZN-2459

Fig. 6

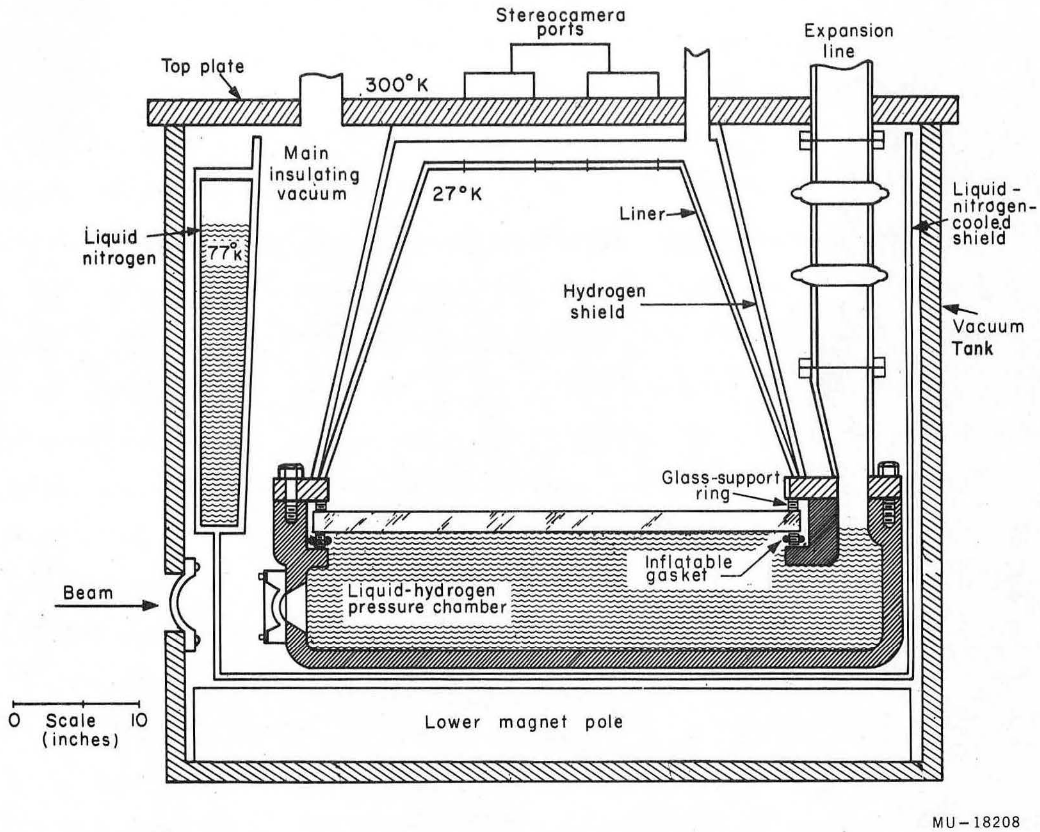
Stereocamera ports
Expansion line
Top plate
300°K
Main insulating vacuum
27°K
Liner
Liquid-nitrogen-cooled shield
Liquid nitrogen
77°K
Hydrogen shield
Vacuum Tank
Glass-support ring
Inflatable gasket
Beam
Liquid-hydrogen pressure chamber
0 Scale 10 (inches)
Lower magnet pole
MU-18208

Fig. 7

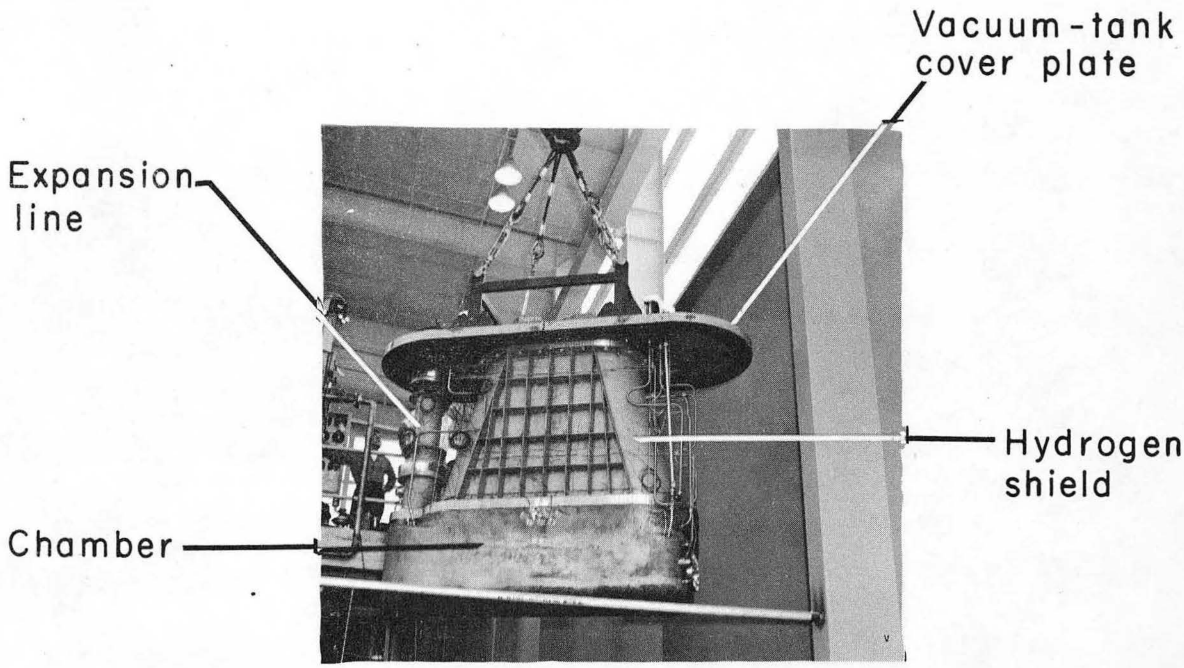
Vacuum-tank
cover plate
Expansion
line
Hydrogen
shield
Chamber

ZN-2460

Fig. 8

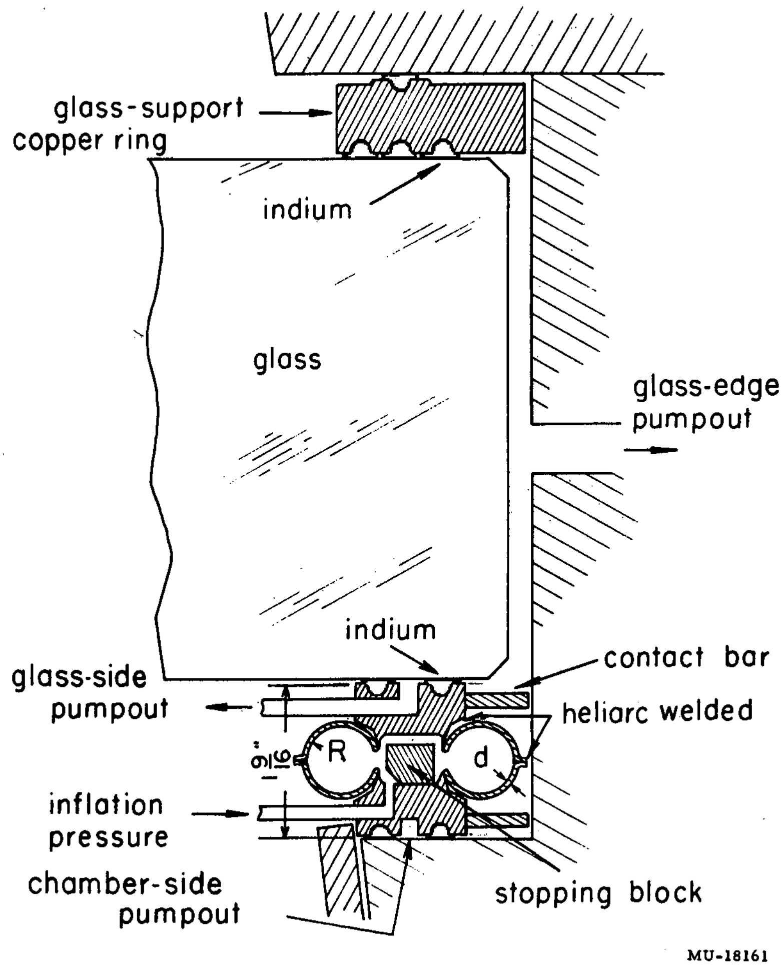
glass-support copper ring
indium
glass
glass-edge pumpout
indium
contact bar
glass-side pumpout
heliarc welded
R
d
9/16"
inflation pressure
chamber-side pumpout
stopping block
MU-18161

Fig. 9

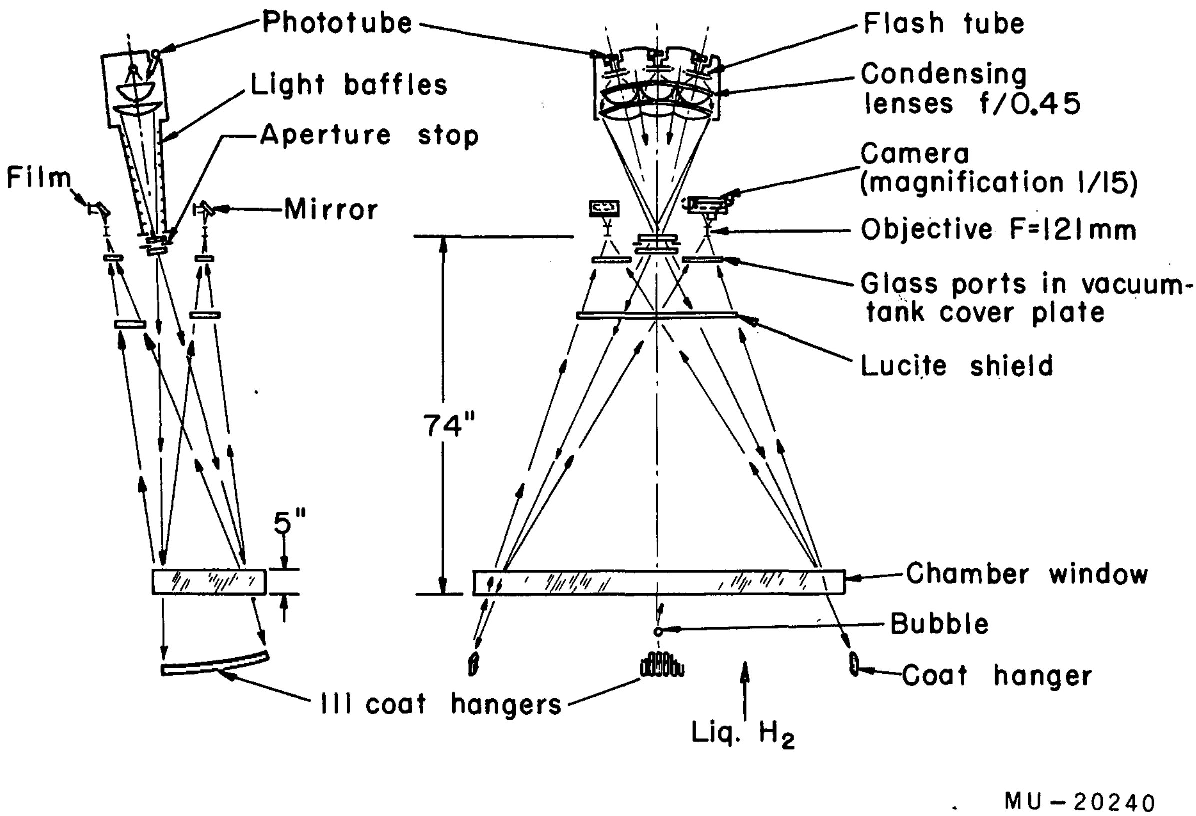
Phototube
Light baffles
Aperture stop
Film
Mirror
5"
111 coat hangers
Flash tube
Condensing lenses f/0.45
Camera (magnification 1/15)
Objective F=121mm
Glass ports in vacuum-tank cover plate
Lucite shield
74"
Chamber window
Bubble
Coat hanger
Liq. H_2
MU-20240

Fig. 10

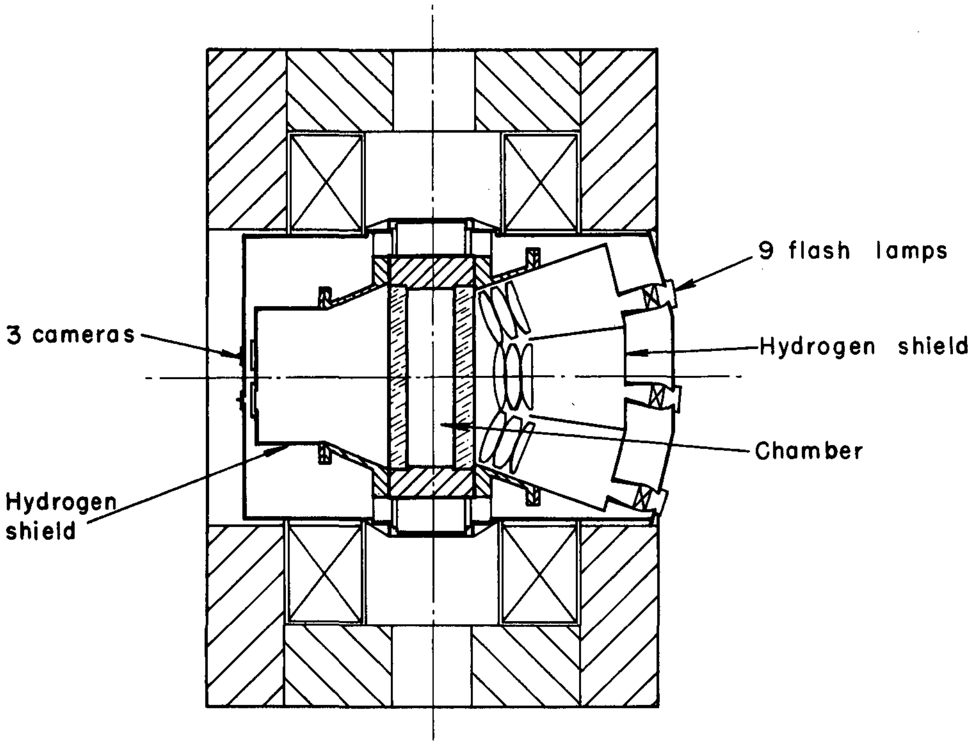

MU-20241

Fig. 11

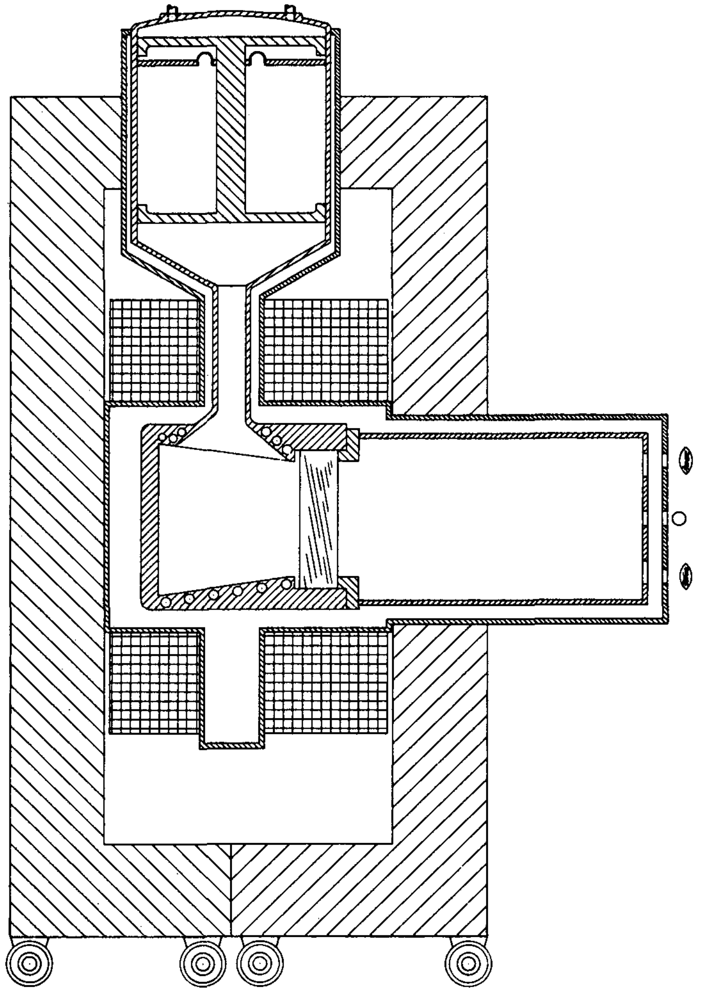

MU—20237

Fig. 12

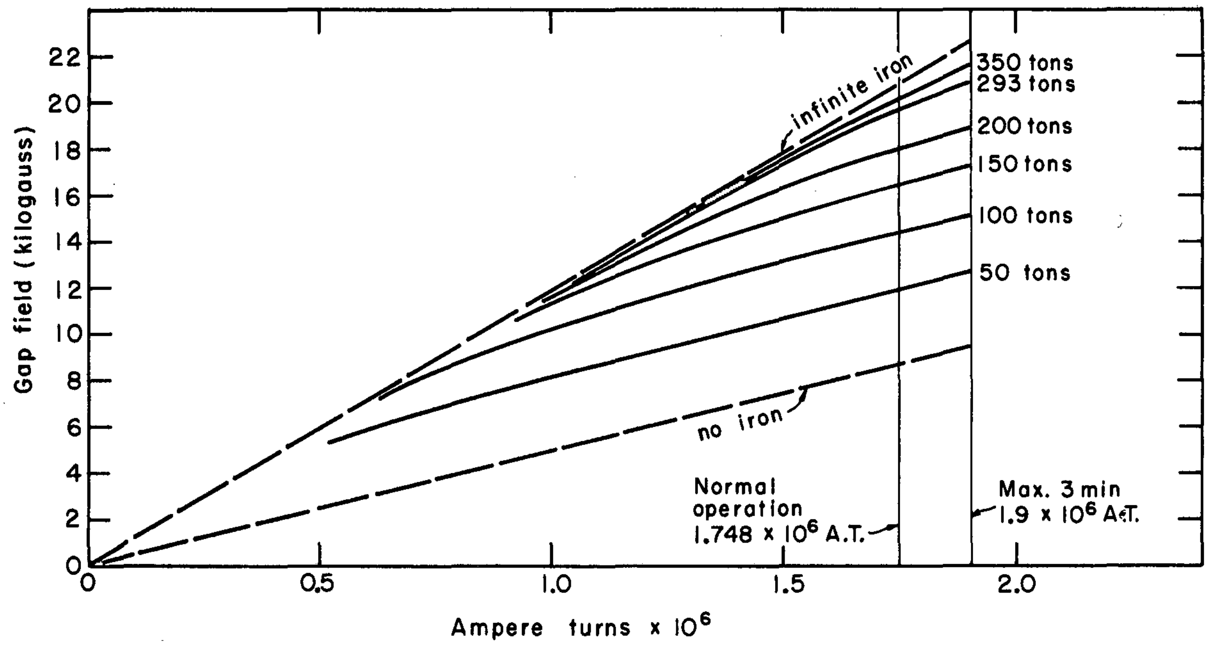
Gap field (kilogauss)
Ampere turns x 10⁶
infinite iron
350 tons
293 tons
200 tons
150 tons
100 tons
50 tons
no iron
Normal operation 1.748 x 10⁶ A.T.
Max. 3 min 1.9 x 10⁶ A.T.
MU-20242

Fig. 13

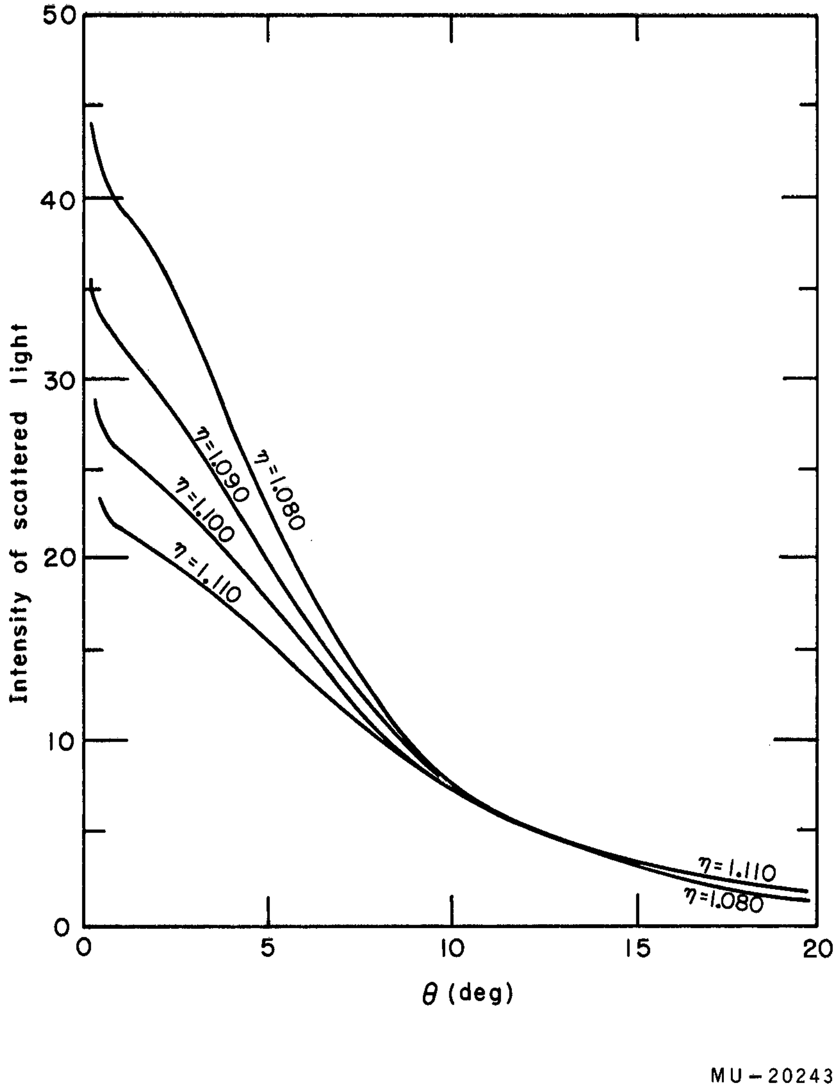
Intensity of scattered light
θ (deg)
0
5
10
15
20
0
10
20
30
40
50
η=1.080
η=1.090
η=1.100
η=1.110
η=1.110
η=1.080
MU-20243

Fig. 14

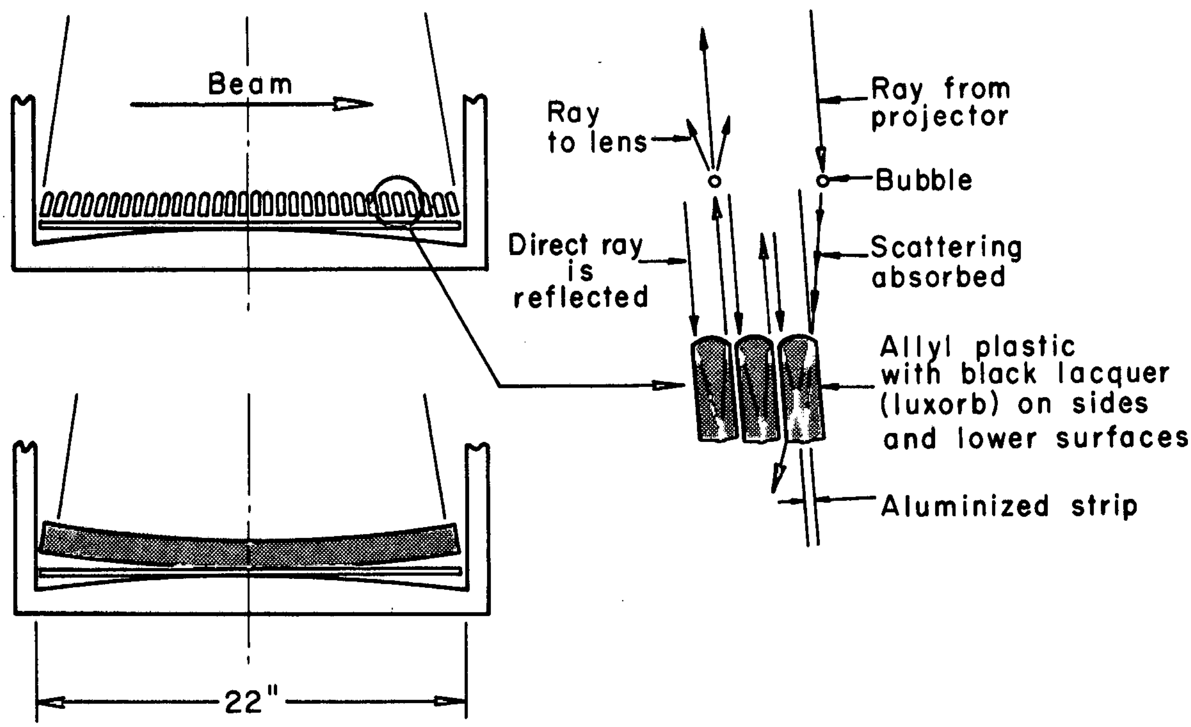

MU-20244

Fig. 15

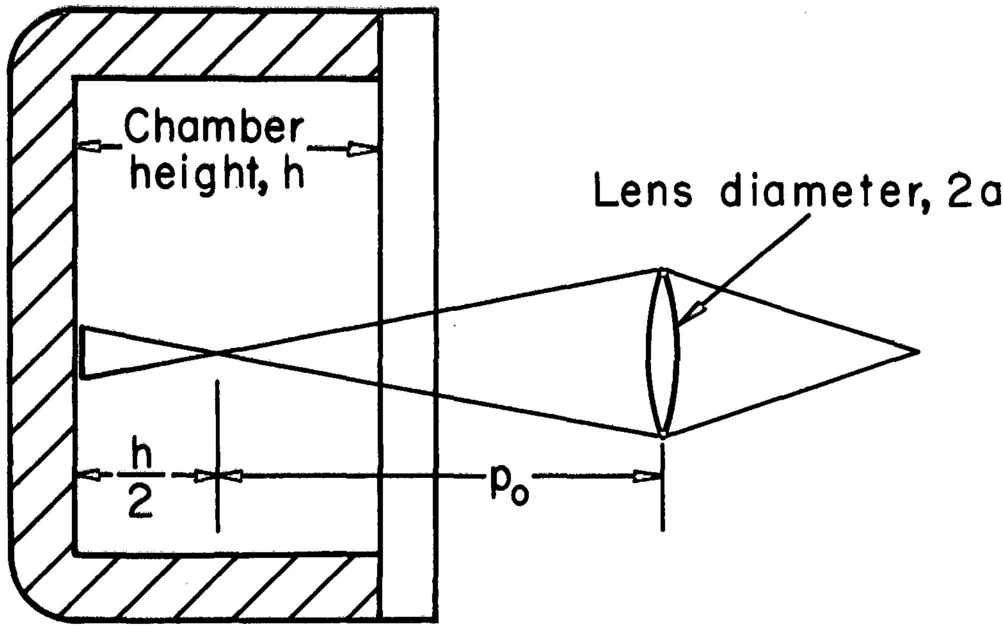

MU-20245

Fig. 16

ZN-2461

Fig. 17

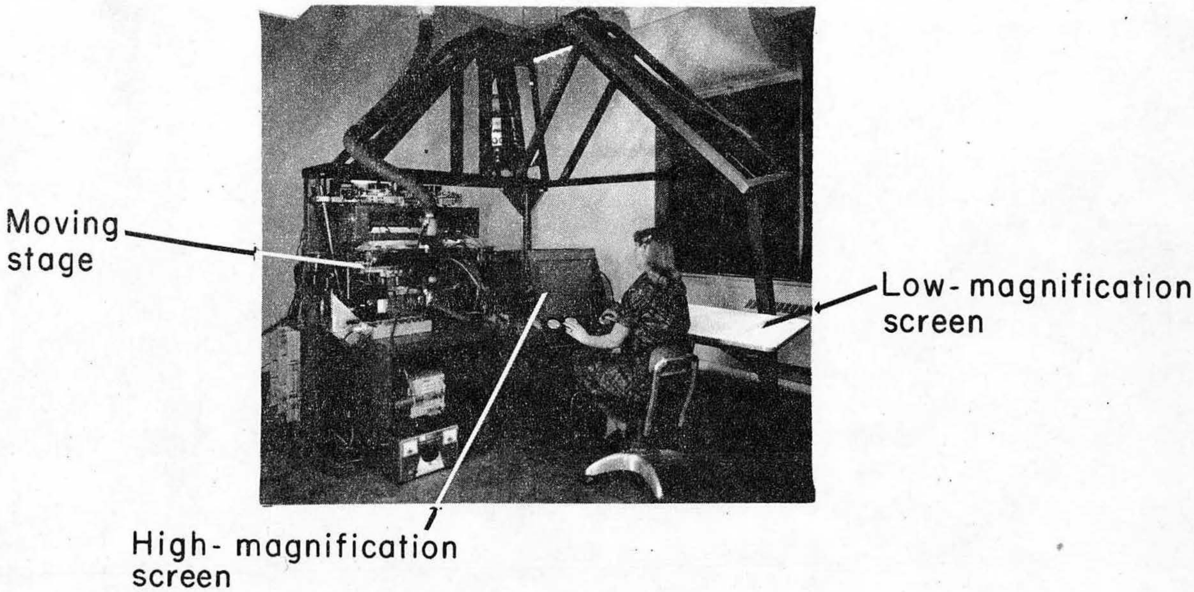

ZN-2462

Fig. 18

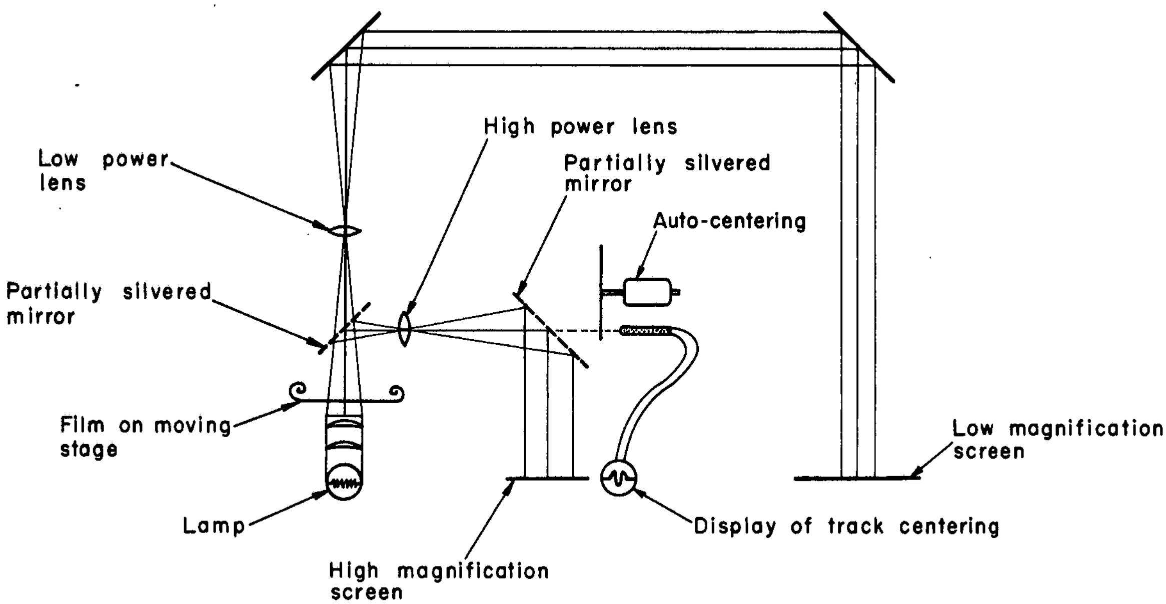

MU-20246

Fig. 19

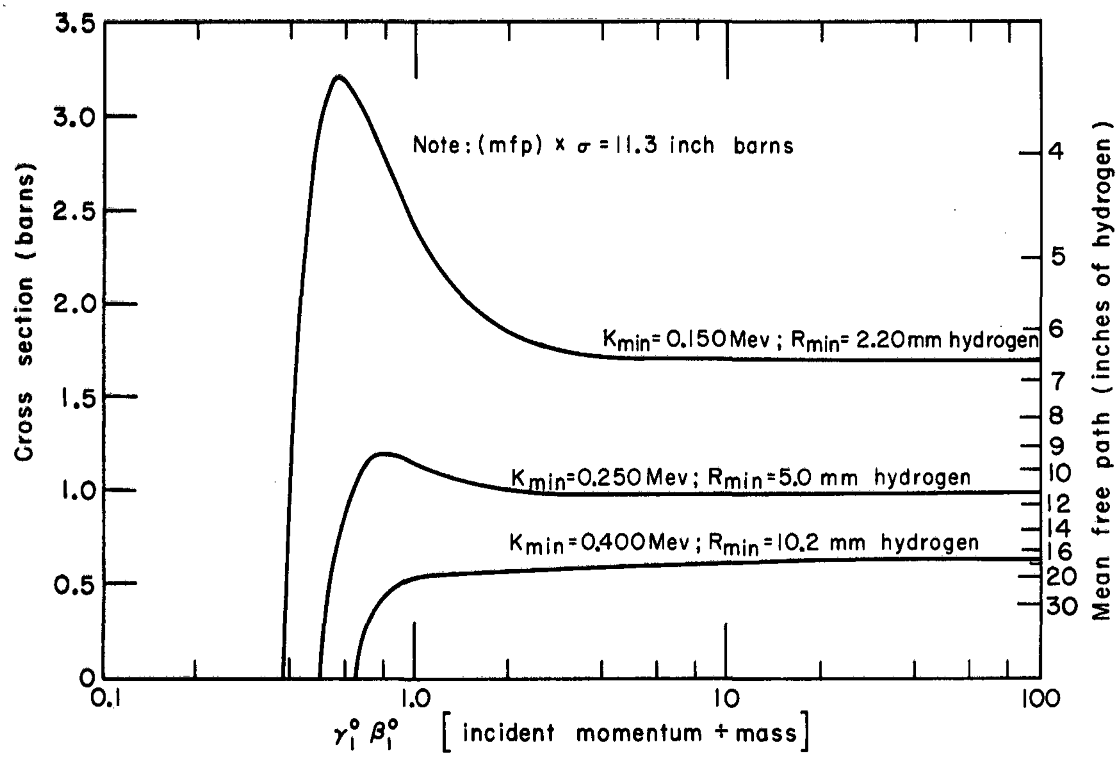

MU-20247

Fig. 20

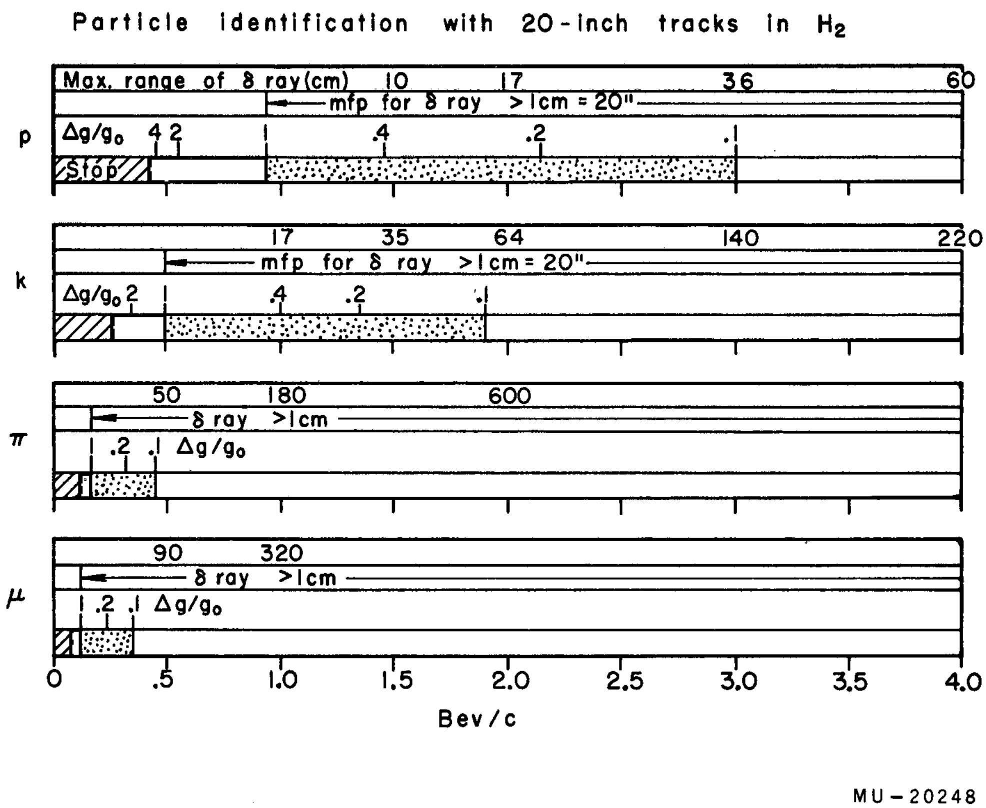
Particle identification with 20-inch tracks in H_2
Max. range of δ ray (cm) 10 17 36 60
mfp for δ ray > 1cm = 20"
p
Δg/g₀ 4 2 1 .4 .2 .1
Stop
17 35 64 140 220
mfp for δ ray > 1cm = 20"
k
Δg/g₀ 2 1 .4 .2 .1
50 180 600
δ ray > 1cm
π
1 .2 .1 Δg/g₀
90 320
δ ray > 1cm
μ
1 .2 .1 Δg/g₀
0 .5 1.0 1.5 2.0 2.5 3.0 3.5 4.0
Bev/c
MU-20248

Fig. 21

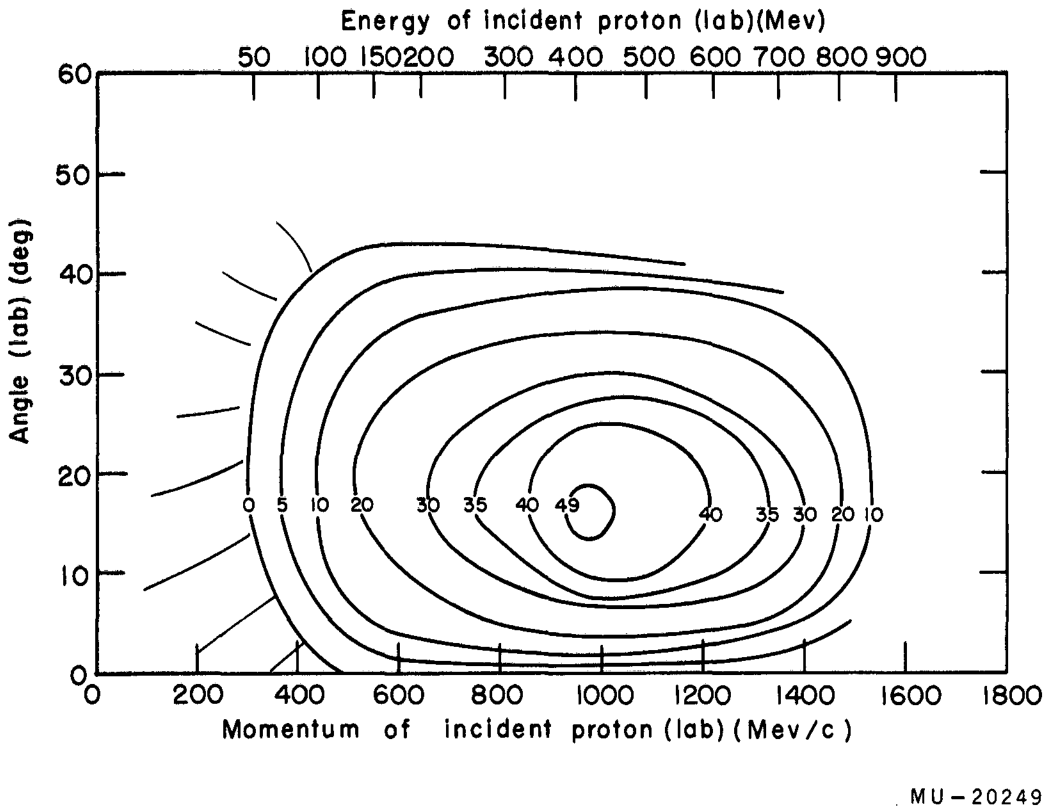
Energy of incident proton (lab)(Mev)
50 100 150 200 300 400 500 600 700 800 900
Angle (lab) (deg)
0 10 20 30 40 50 60
0 5 10 20 30 35 40 49 40 35 30 20 10
0 200 400 600 800 1000 1200 1400 1600 1800
Momentum of incident proton (lab) (Mev/c)
MU-20249

Fig. 22

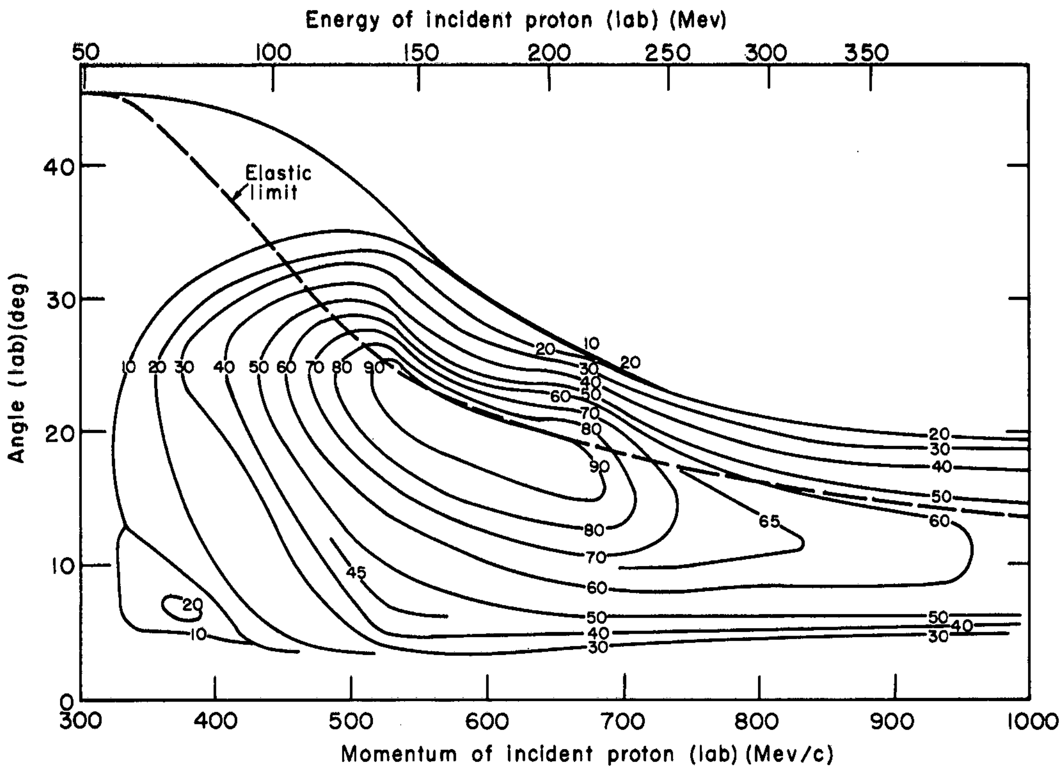

MU-20250

Fig. 23

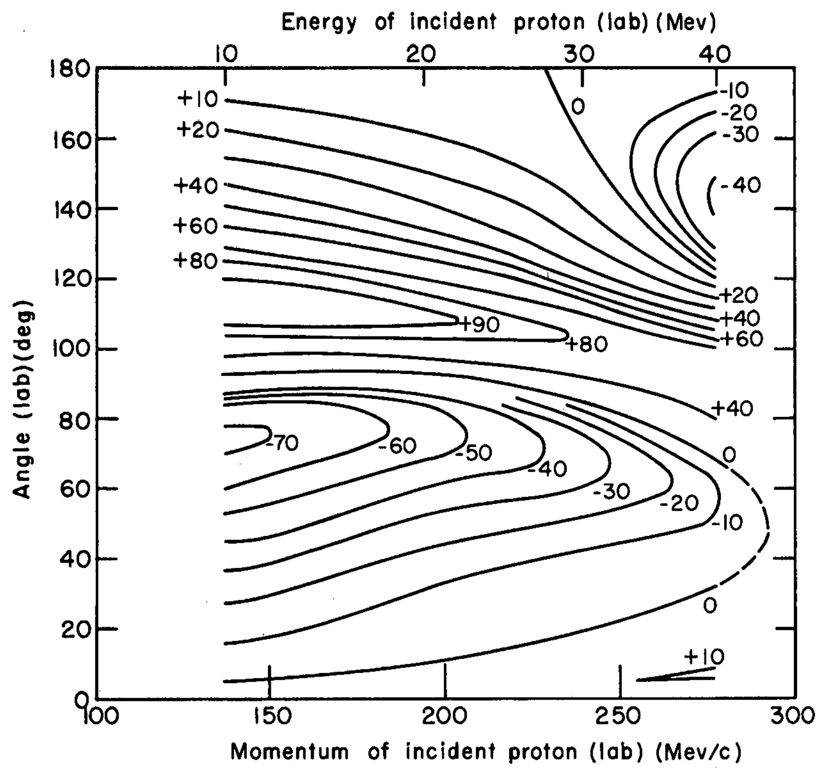

MU-20251

Fig. 24

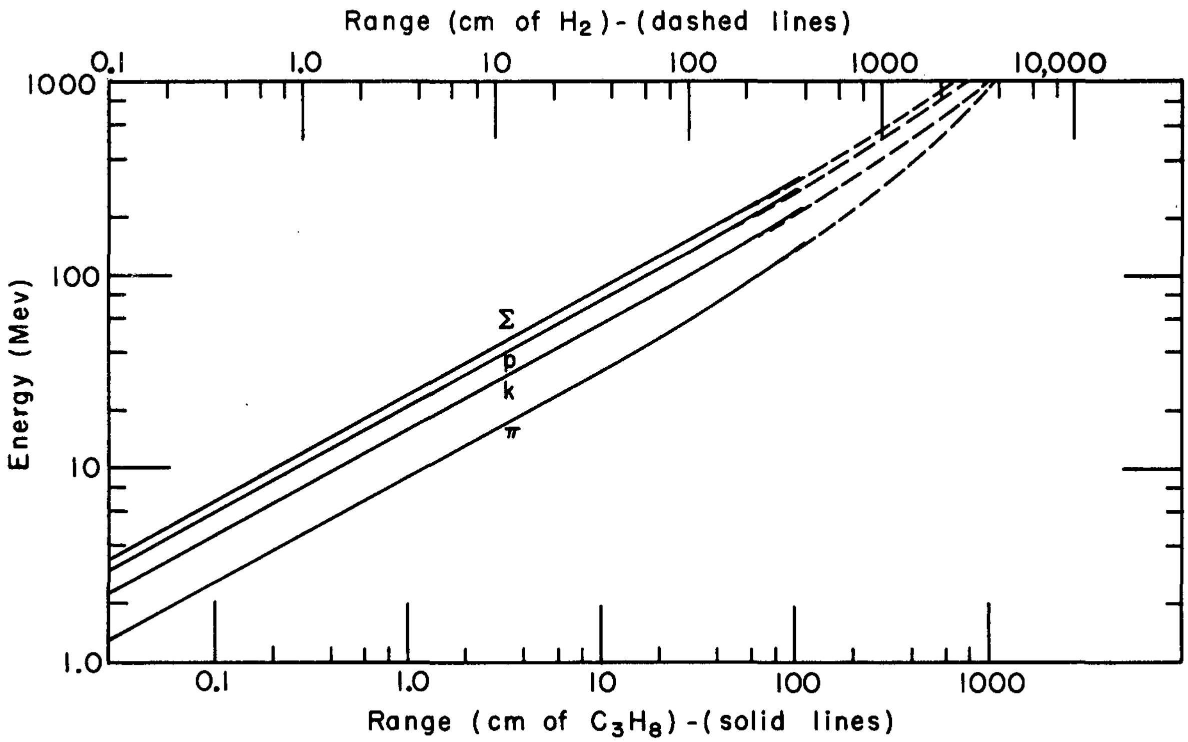

MU-20252

Fig. 25

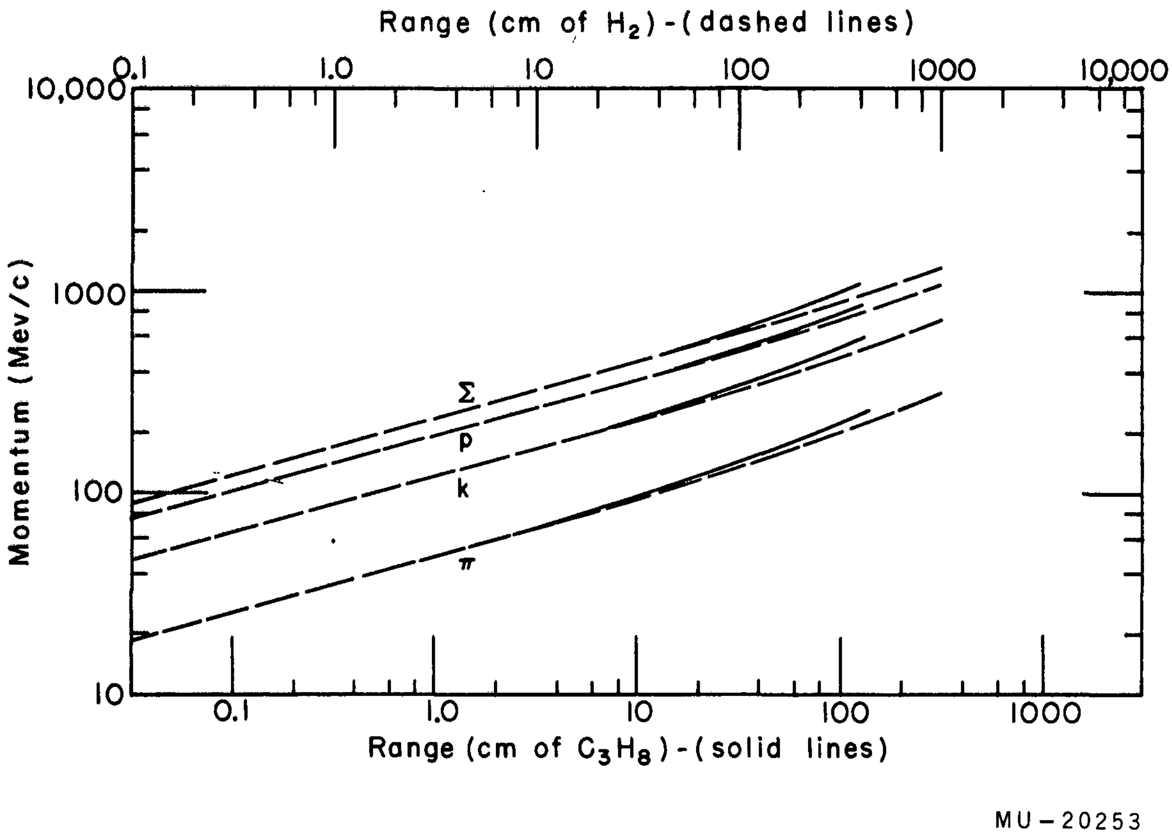
Range (cm of H2)-(dashed lines)
0.1
1.0
10
100
1000
10,000
10,000
1000
100
10
Momentum (Mev/c)
Σ
p
k
π
0.1
1.0
10
100
1000
Range (cm of C3H8)-(solid lines)
MU-20253

Fig. 26